Department of Applied Physics

Fabrication and electrochemical performance analysis of nanocomposite for low-temperature SOFC

Yifu Jing

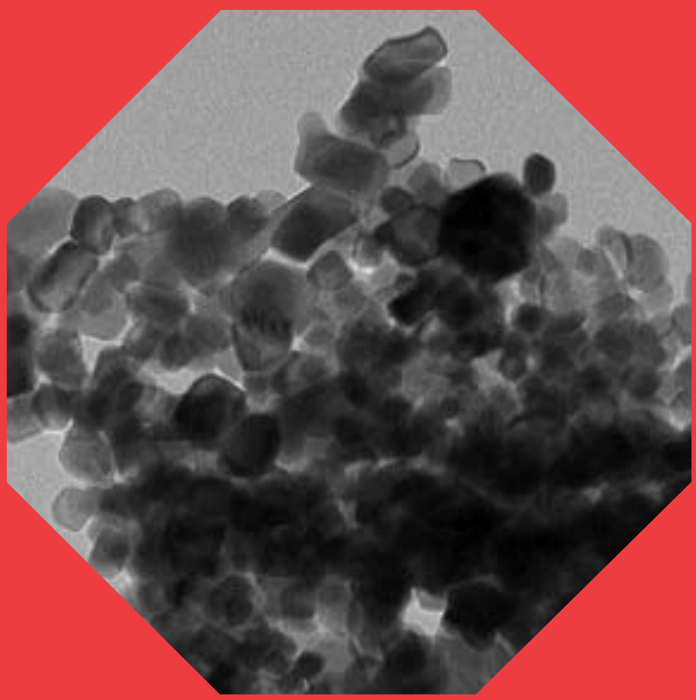

Aalto University

DOCTORAL DISSERTATIONS

Aalto University publication series
DOCTORAL DISSERTATIONS 138/2017

Fabrication and electrochemical performance analysis of nanocomposite for low-temperature SOFC

Yifu Jing

A doctoral dissertation completed for the degree of Doctor of Science (Technology) to be defended, with the permission of the Aalto University School of Science, at a public examination held at the lecture hall M1 of the school (Otakaari1) on 29 September 2017 at 12:00.

Aalto University
School of Science
Department of Applied Physics
New Energy Technologies

Supervising professors
Professor Peter D. Lund
Aalto University, Finland

Thesis advisors
Professor Bin Zhu
Royal Institute of Technology KTH, Sweden
Hubei University, China

Preliminary examiners
Professor Hao Wang
Hubei University, China

Professor Meng Ni
Hong Kong Polytechnic University, Hong Kong

Opponents
Professor Yongdan Li
Tianjin University, China

Aalto University publication series
DOCTORAL DISSERTATIONS 138/2017

ISBN 978-952-60-7538-9 (printed)
ISBN 978-952-60-7537-2 (pdf)
ISSN-L 1799-4934
ISSN 1799-4934 (printed)
ISSN 1799-4942 (pdf)
http://urn.fi/URN:ISBN:978-952-60-7537-2

Unigrafia Oy
Helsinki 2017

Finland

441 697
Printed matter

Author
Yifu Jing

Name of the doctoral dissertation
Fabrication and electrochemical performance analysis of nanocomposite for low-temperature SOFC

Publisher School of Science

Unit Department of Applied Physics

Series Aalto University publication series DOCTORAL DISSERTATIONS 138/2017

Field of research Engineering Physics, Advanced Energy Systems

Manuscript submitted 30 June 2016 **Date of the defence** 29 September 2017

Permission to publish granted (date) 13 October 2016 **Language** English

☐ **Monograph** ☒ **Article dissertation** ☐ **Essay dissertation**

Abstract

Low-temperature solid oxide fuel cell (LTSOFC) offers a promising new energy conversion technology, which converts chemical energy into electrical energy. The benefits of LTSOFC technology include a low operating temperature, relatively high energy conversion efficiency, and potentially low costs. One of the key challenges with LTSOFC, however, is the power density and the ionic conductivity of the electrolyte, which still needs improvement.

In this work, several different synthetic and fabrication processes, such as co-precipitation synthesis, freeze-drying synthesis, and spark plasma sintering (SPS) techniques were employed to enhance the performance of the composite electrolyte for the LTSOFC fuel cell. As the base electrolyte material, samarium-doped ceria (SDC) was employed, which was also modified by adding a carbonate element (CSDC). A LiNiCuZn electrode composite was utilized, which was synthesized using the slurry method. The ionic conductivity of the electrolyte could be improved via the freeze-drying and SPS methods as opposed to the co-precipitation method.

The cold-pressing and hot-pressing methods were separately applied to prepare laboratory unit cells of the LTSOFC with the following results. The highest power density obtained was 1 W/cm^2 at 470 ^{0}C. The best ionic conductivities were obtained by freeze-drying and the SPS, which exceeded 0.4 S/cm. In a carbonate-SDC electrolyte, adding CO_2 to the air oxidant clearly improved the power density and the open circuit voltage of the fuel cell. The power density was improved by 30–100% and the OCV by 0.1–0.2 V compared to using pure air as an oxidant.

Keywords fuel cells, low-temperature SOFC, nanocomposite, ionic conductivity, hydrogen

ISBN (printed) 978-952-60-7538-9 **ISBN (pdf)** 978-952-60-7537-2

ISSN-L 1799-4934 **ISSN (printed)** 1799-4934 **ISSN (pdf)** 1799-4942

Location of publisher Helsinki **Location of printing** Helsinki **Year** 2017

Pages 111 **urn** http://urn.fi/URN:ISBN:978-952-60-7537-2

Preface

The work presented in this thesis has been conducted in the New Energy Technologies (NEW) group, Department of Applied Physics of the Aalto University School of Science, Espoo, Finland from 2012 to spring 2016. Financial support for the work came from the Academy of Finland through the "Single-component fuel cell"-project and from TEKES through the "LTSOFC"-project.

Several people have contributed to the work completed in this thesis. First, my sincerest thanks go to my supervisor, Prof. Peter D. Lund at Aalto University, and my co-instructor, Prof. Bin Zhu at the Royal Institute of Technology KTH, Stockholm and Hubei University, China. Important help also came from my colleagues, Dr. Janne Patakangas, Dr. Ying Ma, Dr. Imran Asghar, Dr. Ghufran Hashmi, Dr. Janne Halme, and Dr. Kati Miettunen. Many thanks also go to the whole New Energy Technologies Group for encouragement during my work.

To my family and especially to my father, elder brothers, and my girlfriend, thank you for your company and always encouraging me to continue this long work. I would not have had this opportunity to study without your help and encouragement.

Espoo, 20.6.2017

Yifu Jing

Contents

Symbols and Abbreviations

Symbols

A’	Area
a_{red}	Activity of the reduced chemicals
a_{OX}	Activity of the oxidized chemicals
E	Voltage
E^o	Standard potential
E_a	Activation energy of reaction
K	Reaction speed constant
R’	Gas constant
F	Faraday constant
L	Length
n	Number of electron transmissions
R	Resistance
T	Temperature (K)
Z’	Real impedance
Z”	Imaginary impedance
Ω	Ohm
σ	Conductivity

θ	Angle between the incident ray and the scattering

Abbreviations

A	Current, Amps
AC	Alternating current
AFC	Alkaline fuel cell
CDC	Calcium-doped ceria
CFC	Ceramic fuel cell
CGDC	Carbonate-gallium-doped ceria
CSDC	Carbonate-samarium-doped ceria
EDS	Energy dispersive X-ray spectroscopy
EIS	Electrochemical Impedance Spectroscopy
FESEM	Field Emission Scanning Electron Microscope
GDC	Gallium-doped ceria
I	Current, amps
LiNiCuZn	$Li_{0.15}Ni_{0.46}Cu_{0.15}Zn_{0.23}O$
LTSOFC	Low temperature solid oxide fuel cell
MCFC	Molten carbonate fuel cell
NSDC	Sodium carbonate-samarium-doped ceria
OCV	Open circuit voltage
PAFC	Phosphoric acid fuel cell
PEMFC	Proton exchange membrane fuel cell

SDC	Samarium-doped ceria
SEM	Scanning electron microscope
SOFC	Solid oxide fuel cell
SPS	Spark plasma sintering
TEM	Transmission electron microscope
V	Voltage, volt
W	Power, watts
XPS	X-ray photoelectron *spectroscopy*
XRD	X-ray diffraction
YSZ	Yttrium stabilized zirconium

List of Publications

This doctoral dissertation consists of a summary and five publications, which are referred to in the text by their numerals:

I. Jing Y., Ma Y., Patakangas J., Zhu B., Johnsson M., Erkin C. M., Lund P. Enhanced conductivity of SDC-based nano-composite electrolyte by spark plasma sintering. *International Journal of Hydrogen Energy*, 39, 14391–14396 (2014).

II. Jing Y., Patakangas J., Lund P., Zhu B. An improved synthesis method of ceria-carbonate based composite electrolytes for low-temperature SOFC fuel cells. *International Journal of Hydrogen Energy*, 38, 16532-16538 (2013).

III. Jing Y., Qin H., Liu Q., Singh M., Zhu B., Synthesis and electrochemical performances of LiNiCuZn oxides as anode and cathode catalyst for low temperature solid oxide fuel cell. *Journal of Nanoscience and Nanotechnology*, 12, 1-5 (2012).

IV. Jing Y., Lund P. Effect of alkali carbonate in SDC electrolyte for nano-composite fuel cell. *Nano Energy Systems*, 1(1), 22-28 (2017).

V. Patakangas J., Jing Y., Asghar, M.I., Lund P. Investigation of LiNiCuZn-oxide electrodes prepared by different methods: synthesis, characterization and properties for nanocomposite fuel cells. *International Journal of Hydrogen Energy*, 41(18), 7609–7613 (2016).

Author's Contribution

Publication I: Enhanced conductivity of SDC-based nano-composite electrolyte by spark plasma sintering

The author synthesized the LiNiCuZn electrode by the slurry method, and the SDC-carbonate electrolyte materials by the co-precipitation method from nitrate and carbonate chemicals. The author fabricated the fuel cells by the cold-pressing method and measured the cells. The EIS and XRD were completed in cooperation with the co-authors. The author participated in the writing of the publication.

Publication II: An improved synthesis method of ceria-carbonate based composite electrolytes for low-temperature SOFC fuel cells

The author synthesized the CSDC electrolyte with the freeze-drying method. The author cooperated with the co-authors on the EIS and XRD measurements. The SEM and mapping measurements were carried out by the author. The author participated in the writing of the publication.

Publication III: Synthesis and electrochemical performances of LiNiCuZn oxides as anode and cathode catalyst for low temperature solid oxide fuel cell

The author had primary responsibility for all parts of the publications except the SPS process. The electrolyte samples for the SPS process were prepared by author. The author participated in the writing of the publication.

Publication IV: Effect of alkali carbonate in SDC electrolyte for nano-composite fuel cell

The author had primary responsibility for all parts of the publication. The author synthesized the electrode and electrolyte materials. The author manufactured the electrode and electrolyte membrane, and the LTSOFC fuel cell through the hot-pressing method. The gas mix and supply device was designed by the author. The author did all electrochemical performance measurements. The author participated in the writing of the publication.

Publication V: Investigation of LiNiCuZn-oxide electrodes prepared by different methods: synthesis, characterization and properties for nanocomposite fuel cells

The author had primary responsibility for materials synthesis and fuel cell fabrication. The author participated in the writing of the publication.

Other publications by the author

Lund P., Hashmi G., Ma Y., Patakangas J., Jing Y. Degradation and stability of nano-structured energy devices. Microelectronic Engineering, 126, 49-53 (2014).

Patakangas J., Ma Y., Jing Y., Lund P. Review and analysis of characterization methods and ionic conductivities for low-temperature fuel cells (LT-SOFC). Journal of Power Sources, 263, 315-331 (2014).

Qin H., Zhu B., Liu Q., Jing Y., Raza R. ,Syedkhalid I., Manish S., Ghazanfar G., Zhu B. Direct biofuel low-temperature solid oxide fuel cells. Energy & Environmental Science, 4, 1273-1276 (2011).

1. Introduction

1.1 Background

Fossil fuels have been key to human development, enabling the growth of the modern advanced society with its high standard of living. At the same time, the utilization of fossil fuels have caused adverse effects, such as the energy crisis, greenhouse effect, ozone hole, and other environmental pollution and damage [1]. As these effects may jeopardize ecosystems and economic well-being [2, 3], the development of clean energy alternatives to fossil fuels has become both a necessary and urgent task.

Clean energy sources include different forms of renewable energy, such as hydro power, wind power, solar energy, bio-energy, tidal energy, and ocean thermal energy [4]. However, their utilization in global energy consumption remains relatively low at around 19% of global energy consumption in 2015 [5]. Around the world, many concerned countries have been implementing new initiatives to promote the use of clean energy. The Europe Union aims, for instance, to raise the scale of renewable energy to 20% of its energy consumption by 2020 [6]. As demand for clean energy grows, there has been considerable interest in new research developments in promising alternatives; chief among these are hydrogen energy technologies, which employ hydrogen as an energy carrier, fuel, and storage. In theory, hydrogen could form the basis of a future global energy system. Hydrogen is often associated with high-efficiency energy conversion technologies, such as fuel cells, which convert chemical energy into electricity through electrochemical reactions without any moving parts [7]. Fuel cells provide high energy conversion efficiency and high power density, without producing any noise or pollution [8]. Consequently, fuel cells and hydrogen

energy have garnered substantial interest worldwide; for instance, they featured prominently in China's 12th 5-year plan for 2011–2015 [9].

Although often regarded as a relatively recent invention, fuel cells were in fact invented in the 19th century. However, their first true success came much later with their application in space programs, such as the Apollo program [10]. Fuel cells are also employed in submarines due to their inherent noiseless performance [11]. Interest in fuel cells grew substantially during the energy crises of the 1970s, which in turn led to major technology developments and deployment efforts. Since then, fuel cells have successfully been demonstrated as small-scale power plants and in vehicular uses. As it stands today, fuel cells are employed in different niche applications, but they are not yet fully commercial in mobile and stationary applications. Their relatively high costs and durability concerns remain the key challenges ahead for fuel cells.

Currently, there are several types of fuel cells, which provide an array of different characteristics. The solid oxide fuel cell (SOFC) is an interesting technology as it is based on a solid ion conductor and employs low-cost ceramic or metallic materials [12]. As the SOFC operates at a high temperature to provide adequate ionic conductivity, a range of fuels could also be employed through auto-thermal reforming of fuels into hydrogen and carbon monoxide, which can both be employed in the SOFC [13-15]. Other advantages of the SOFC are its high power and current density.

The SOFC fuel cell has a high operating temperature (700–1000 ^{o}C) which leads to major durability issues and requirements on materials, gas sealing, and so forth [16-17]. To overcome these challenges, one strategy would be to lower the temperature; however, this would necessitate changing the electrolyte to maintain a sufficiently high ionic conductivity, which is important for fuel cell performance. In a low temperature solid oxide fuel cell (LTSOFC), the required temperature is only 300–600 ^{o}C. However, with advanced material solutions, such as samarium-doped ceria as the electrolyte, it is still possible to achieve an effective ionic conductivity [18–19]. The relatively low operating temperature of the LTSOFC can ease the choice of materials, which may likewise decrease the costs.

1.2 Motivation and objectives of this thesis

Although the LTSOFC technology shows promising properties, several problems remain before this technology can be commercialized. Many of the open issues are related to the performance of the LTSOFC and its components, and in particular to the utilized materials. Thus, this thesis focuses on the material selection for and the fabrication of the LTSOFC in order to identify solutions to improve its performance.

The LTSOFC is often based on doped cerium oxide including samarium-doped ceria (SDC), gallium-doped ceria (GDC), and calcium-doped ceria (CDC) [20–23]. The cerium-based electrolyte has high ionic conductivity at low temperatures. Recently, the ionic conductivity has been improved by employing nanostructures, such as nano-composites made of carbonates and SDC (CSDC). For the electrodes, low cost metal oxides like nickel oxide, zinc oxide, and copper oxide have been employed as well as different kinds of carbonate salts [24]. These developments have led to the LTSOFC achieving a power density of 1000 mW/cm^2 at 470 ^{0}C and 1700 mW/cm^2 at 650 ^{0}C [25].

Accordingly, this study aims to build on this success by further developing the LTSOFC through improved material synthesis of nano-composites, mainly that of the electrolyte, but also through the oxidant content and fabrication of the fuel cells. Different material synthesis methods were chosen to improve the performance of both the electrode and electrolyte. The materials for the electrodes were synthesized with the slurry and solid mixing methods. For the electrolyte material synthesis, the co-precipitation, freeze-drying, and spark plasma sintering (SPS) methods were utilized. Fuel cell fabrication methods and different oxidants were also applied for the LTSOFC.

The structure of this thesis is as follows. Chapter 1 provides a general introduction, background, and motivation for further developing low temperature SOFC. Chapter 2 presents the fuel cell principle along with the different fuel cell technologies. Thereafter, the experimental methods utilized in the thesis are described in Chapter 3. The main results of these experiments are

presented in Chapter 4 and are divided into subsections according to the aforementioned journal publications. Finally, Chapter 5 includes a summary and the conclusions of this thesis.

2. Fundamentals of a fuel cell

2.1 Basic working principle of fuel cell

A fuel cell converts chemical energy into electrical energy though the oxidation-reduction reaction [26]. The fuel on the anode side is oxidized into ions on the surface of a catalyst (electrode) and releases electrons, which are employed in an external circuit and then returned to the cathode, where the oxidant is reduced into ions [27]. The ions created in the electrochemical reaction will transfer through the electrolyte layer. The specific type of ions depends on the type of the fuel cell (e.g. H^+, O^{2-}, CO_3^{2-}, OH^-, and PO_4^{3-}). Regardless of the ion types, there is always an electrical balance between the ions through the internal circuit and electrons through the external circuit.

In Fig. 2.1, the cross section of a fuel cell illustrates its key components, that of an anode, cathode, and electrolyte. The electrode of the fuel cell is also a catalyst. The electrode is normally a mixed electrode composed of pure electrode and electrolyte [29-31] to allow for both ionic and electronic conductivity.

The electrolyte is utilized to separate the anode and the cathode to avoid short-circuiting, and it forces the electron to transmit through the external circuit. Attached to the anode and cathode, the current collector is used to gather the created current.

Here, it is worth considering a solid oxide fuel cell (SOFC) with hydrogen as the fuel and oxygen as the oxidant. The reduction and oxidation reactions are the following [32–33]:

Anode reaction: $H_2 - 2e^- \rightarrow 2H^+$ (1)

Cathode reaction: $O_2 + 4e^- \rightarrow 2O^{2-}$ (2)

Overall reaction: $H_2 + 1/2O_2 \rightarrow H_2O$ (3)

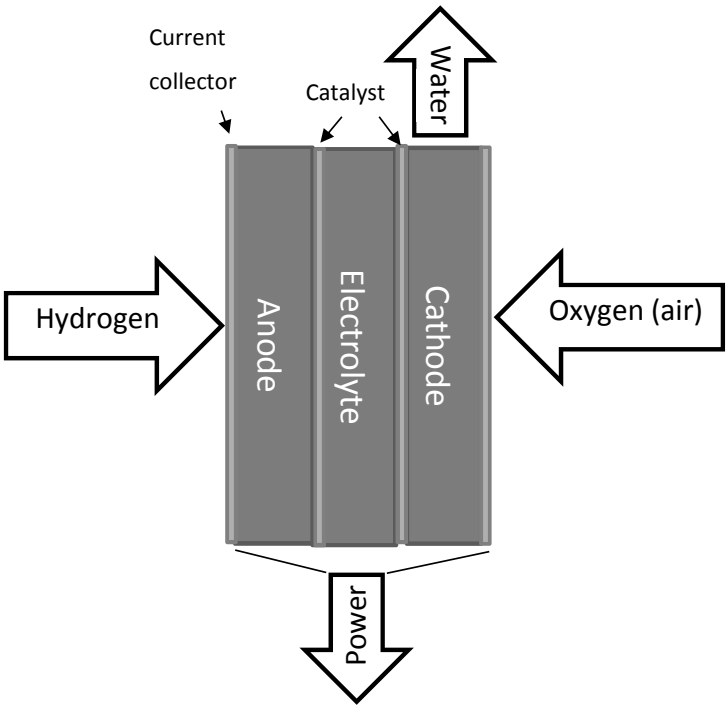

Figure 2.1. Structure of a fuel cell, the anode (negative electrode) receives the fuel (hydrogen) and the cathode (positive electrode) the oxidant (air/oxygen).

The operating temperature of the fuel cell displayed in Table 2.1 affects the ionic conductivity of its electrolyte. If the fuel cell temperature is sufficiently high, then less catalyst will be necessary. However, a lower operating temperature requires a catalyst with a higher catalytic activity, according to the Arrhenius equation in Eq. (4) [34]:

$$K \sim e^{-E_a/R'T} \quad (4)$$

where K is the reaction speed constant; E_a is the activation energy of reaction; R' is the gas constant; and T is the temperature.

The PEM fuel cell operates at a low temperature of under 100 °C. The SOFC has the highest operating temperature of around 800 °C, followed by the molten carbonate fuel cell (MCFC). In comparison, the LTSOFC has a temperature below 600 °C.

The theoretical ideal voltage, E, of a fuel cell can be calculated by the Nernst equation [35–36]:

$$E = E^0 - \frac{R'T}{nf} ln \frac{a_{red}}{a_{OX}} \qquad (5)$$

where E^0 is the standard potential; R' is the ideal gas constant, 8.314472(15) $J.K^{-1}.mol^{-1}$; T is the temperature (K); F is the Faraday constant; n is the number of electron transmissions in the semi reaction formula (mol); a_{red} is the activity of the reduced chemicals; and a_{OX} is the activity of the oxidized chemicals.

Once current is drawn for the fuel cell, voltage losses will occur through activation, ohmic, and concentration potential losses, or so-called polarization, which decrease the performance of the fuel cell [37]. Figure 2.2 illustrates the losses. The theoretical voltage in Eq. (5) represents the highest possible voltage, but the activation required at the electrode will drop the voltage at I = 0 called the Open Circuit Voltage (OCV) to a lower value. The ohmic, or resistive, losses originate mainly from the electrolyte and depend on its conductivity when the fuel cell draws more current. These losses are also addressed in this thesis.

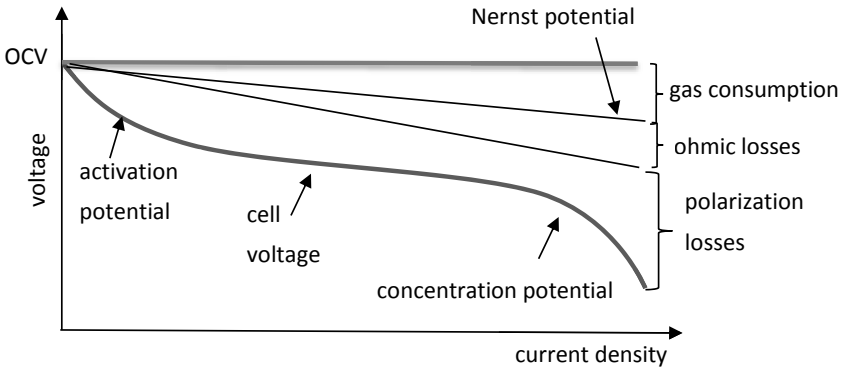

Figure 2.2. Schematic plot of voltage versus current density showing different types of polarizations [37].

2.2 Fuel cell types

There are several types of fuel cells, often named according to the ions involved in the electrochemical reactions. The main fuel cell types are explained in Table 2.1. Typically, fuel cells utilize air or O_2 as oxidants.

The next section provides a short description of the main fuel cell types.

Table 2.1. Fuel cell types and their basic characteristics [38–39].

Name	Type	Electrolyte/ Ions	Oper. temperature （℃）	Electro-chemical efficiency	Fuel	Typical output
AFC	Alkaline fuel cell	KOH solution /OH-	90	50–60%	H_2	300W–5kW
PEMFC	Proton exchange fuel cell	Proton exchange membrane /H^+	80	40–60%	H_2	1kW
PAFC	Phosphoric acid fuel cell	Phosphoric acid / H^+	160–220	45–55%	CH_4, H_2	200kW
MCFC	Molten carbonate fuel cell	Alkali metal carbonates molten mixture/CO_3^{2-}	620–660	50–60%	CH_4, H_2	2MW–10MW
SOFC	Solide oxide fuel cell	Ion conducting ceramic/O^{2-} (H^+)	800–1000	50–65%	CH_4, H_2	1–100kW

i. Alkaline fuel cell (AFC)

The AFC utilizes an amianto network as its carrier electrolyte to support the potassium hydroxide (KOH) solution electrolyte, and it has an operating temperature of 60–200 ℃ [40]. High concentrations of potassium hydroxide (85%) are chosen as the electrolyte at high temperatures (~ 200 ℃), and low

concentrations of potassium hydroxide (35 to 50%) are chosen at low temperatures (< 120 ℃). Compared with other fuel cells, AFC has a higher power density and more reliable performance. However, the AFC must utilize pure hydrogen as the anode of the fuel gas and pure oxygen as the cathode oxidant, and precious metals, such as platinum, gold, and silver, and transition metals, such as nickel, cobalt, and manganese are used as catalysts [41-42]. Unfortunately, the corrosiveness of the AFC electrolytes results in a relatively short lifespan. This characteristic has limited the development of the AFC and relegated its successful use to aerospace or military applications. Thus, it is already lagging behind current technology and is not suitable for development in wider consumer applications.

ii. Proton exchange membrane fuel cell (PEMFC)

The electrolyte for the PEMFC is a solid polymer membrane with strong proton conductivity. Within the PEMFC, water is the only liquid and is non-corrosive; however, water management becomes an important factor affecting the efficiency of the fuel cell. The PEMFC must operate under a water production rate substantially higher than its evaporation rate to ensure the PE film holds adequate water content. The operating temperature of the PEM fuel cell must be limited to below 100 ℃ because of this water balance; however, the operating temperature of the high temperature PEMFC has been shown to reach 180 ^{o}C [43–45]. Normally, the PEMFC operation temperature is about 80 ℃ with a low remaining heat utilization, but it also makes the PEMFC operation start-up time short, which can reach full load in a few minutes [45–47]. Moreover, compared with other liquid electrolytes, such as the phosphoric acid fuel cell (PAFC) and MCFC fuel cell, the PEMFC has a higher current density and specific power, and it has a power generation efficiency of about 43–58%. Its characteristics of long life and reliable operation make it popular for current vehicle power, mobile power, distributed power, and household power supply but not for larger capacity and medium-sized power plants [48].

iii. Phosphoric acid fuel cell (PAFC)

In the PAFC, the phosphate ion conductivity is relatively poor at low temperatures, and the platinum anode is susceptible to the presence of carbon monoxide; thus, the operating temperature of the PAFC is about 160–220 ℃. In addition, the PAFC utilizes a concentration of 100% phosphoric acid as an electrolyte to reduce the pressure of water vapor and improve water management. The phosphoric acid electrolyte is not affected by the presence of carbon dioxide in the fuel gas and air, which is one of the reasons for its first terrestrial applications or its utilization in commercial fuel cells. While the power generation efficiency of the PAFC is only 40–45%, the PAFC technology is mature and already has a market with existing commercial products for decentralized power supply, field mobile power, and backup power supplies [50].

iv. Molten carbonate fuel cell (MCFC)

The MCFC electrolyte is distributed in a porous ceramic material, alkaline carbonate ($LiAlO_2$). This electrolyte has a high ion conductivity when in a molten state at 600–800 ^{o} C. Due to the high operating temperature, nickel and nickel oxide were used as the anode, and the cathode catalyst instead of a noble metal catalyst, such as platinum electrodes, is not necessary for MCFC. Consequently, CH_4 and CO can serve directly as a fuel for the MCFC according its internal reforming capability, which not only improves the efficiency of power generation but also simplifies the system. The power generation capacity and efficiency of MCFC is further improved if combined with the recoverable waste heat with a gas turbine or a combination of complex power systems. Compared with the SOFC, the MCFC has several advantages, such as lower operating temperatures, lower cost metal material, less expensive electrode and electrolyte membrane, simple bipolar plate production and seal technology, low cost and easy to scale power generation [50-51]. The MCFC has some disadvantages though in that the carbon dioxide circulating system must be formulated; it has a shorter life expectancy compared with the SOFC; the molten carbonate is corrosive and volatile; and the power generation efficiency is lower than the SOFC. Compared with the low temperature fuel cells, the long start-up time for the MCFC is not suitable as a backup power supply. Overall, the MCFC is nearing commercialization, and it represents an ideal choice for dispersion stations with centralized power plants.

v. Solid oxide fuel cell (SOFC)

The SOFC electrolyte is a solid-state, non-porous metal oxide, such as Samarium-doped Cerium (SDC) and YSZ (yttria oxide incorporation of zirconium, Y_2O_3-stabilized-ZrO_2), with an operating temperature range of 650–1000 ^{0}C and a high oxygen ionic conductivity [52,54]. Generally, the anode is constituted from ceramic material, such as cobalt or nickel-zirconium oxide (Co- ZrO_2 or Ni- ZrO_2), and the cathode is made from manganese-lanthanum strontium (Sr-doped-LaMnO3). The SOFC has a more flexible shape since the electrolyte is solid; thereby, it can be molded into a tubular shape and offset shape. Compared with liquid electrolyte fuel cells (AFC, PAFC, and MFC), the SOFC eliminates problems of electrolyte corrosion and evaporation and offers a long continuous operating life of up to 70,000 hours [53]. However, it is not easy to create a seal between the metal and ceramic materials due to the high operating temperatures. Compared with the low temperature fuel cells, the SOFC has a longer start-up time, which is not suitable as an emergency power source. Compared with the MCFC, the SOFC provides higher efficiency and a longer life gas turbine combined with a cycle power generation system. However, it is more difficult to develop the SOFC technique, and the cost remains higher than the MCFC. Overall, the SOFC is an ideal choice for fossil fuel power generation technology in the future from the perspective of plant performance, both for small- and medium-capacity decentralized power supply and large-capacity centralized plants.

2.3 Low temperature solid oxide fuel cell (LTSOFC)

In an SOFC, both the electrode and the electrolyte (YSZ) materials are composed of metal oxides with a high operating temperature (700–1000 ^{0}C). The high operating temperature represents one of the main problems in commercializing the SOFC. The high temperature places heavy requirements on the materials and cell seals. Thus, lowering the operating temperature is one crucial aspect for improving the commercial viability of the SOFC [56].

Both the electrode and electrolyte of the low temperature solid oxide fuel cell (LTSOFC) are composed of low temperature ceramic materials operating at a lower temperature of 300–600 ^{o}C [57–58]. The electrode is formed from a low-cost metal oxide, e.g. ZnO or NiO, and the electrolyte is made from materials, such as Samarium-doped ceria (SDC) with carbonate (CSDC) or carbonate-GDC. The fuel for LTSOFC is H_2, and the oxidant is air, pure O_2, or air and CO_2 [14–15]. The ionic conductivity of the LTSOFC electrolyte is higher at lower temperatures than that of the SOFC electrolyte at higher temperatures [59, 60].

To explain the ionic transmission in a typical LTSOFC, e.g. based on samarium-doped ceria (SDC), the material "doping" theory is often employed [59, 61]. In this theory, the matrix lattice of SDC is CeO_2, and the chemical valence of the cerium ion is +4. When two Sm^{3+} ions have a similar volume but smaller chemical valence than two Ce^{4+}, the positive ions in SDC loose two chemical valences. In order to maintain the balance of electric charge in the SDC lattice between positive ions (Ce^{4+} and Sm^{3+}) and negative ions (O^{2-}), one O^{2-} must be removed from the lattice, then there will be one oxygen ion vacancy created. After doping SDC, the content of samarium ions may reach 20% of all positive ions in the SDC, generating plenty of vacancies.

The electrolyte of a nano-composite, composed of carbonate and SDC, GDC, or CDC, have multiple ion transmission characteristics. The ions could include, in this case, H^+, O^{2-}, and CO_3^{2-}, [62]. In one theoretical explanation, the oxygen ion is transmitted on the interface between the carbonate and the electrolyte [59, 63, 64], also called the interfacial conduction. The interfacial conduction theory is illustrated in Fig. 2.3 to explain dual-ion (H^+ and O^{2-}) transmission. For H^+ transport, the "swing model" has also been proposed [65]. The scheme for CO_3^{2-} transmission is often described as ternary ionic conduction [23, 62]. In our study (Publication IV), we also found an ionic conduction contribution from alkali ions and CO_3^{2-} in a nano-composite LTSOFC.

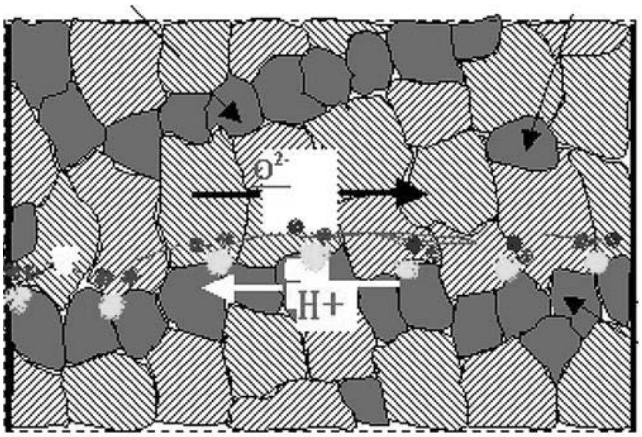

Figure 2.3. A schematic for the proposed hybrid H^+/O^{2-} ion conductor model [67]. Reproduced with permission. Copyright 2013 Elsevier.

A recent further development of the LTSOFC includes the so-called single component fuel cell principle in which a homogenous layer of semiconducting and ionic conducting materials can realize a fuel cell [68].

2.4 Materials for LTSOFC

To decrease the operating temperature while maintaining high ionic conductivity, nano-composite materials including electrode materials and electrolyte materials were investigated in this study. The term, nano-composite, refers to the particle size of the utilized powder materials, which is in the nanometer scale, typically 10–20 nm. At this scale, the surface effect becomes important, e.g. 90% of the atoms will lay on the edge of the particle when its size is < 10 nm. In this thesis, the nano-composite was formed as a 50–100 nm cluster of nanoparticles. The on-edge atoms have a high energy and easily interact with atoms from other materials. The activated and unstable atoms on the surface have high mobility resulting in high ionic conductivity, or so-called super-ionic conductivity [61]. In this work, the nano-composite was composed of carbonate and SDC particles with an interface between the carbonate and SDC as shown in Fig. 2.4 [63].

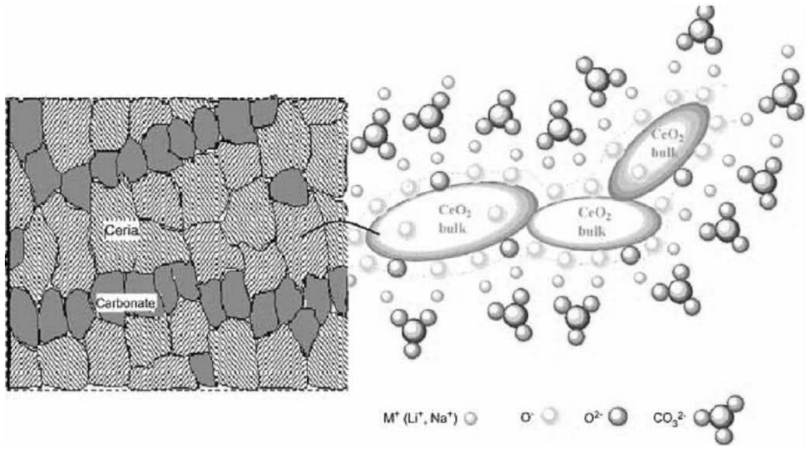

Figure 2.4. Ionic conductivity highway in SDC-carbonate nano-composite electrolyte [63]. Reproduced with permission. Copyright 2008 Elsevier.

Thus, the nano-composites make use of interfaces and interactions in the interfacial regions between the two constituent phases, which result in interfacial ionic conduction highways, i.e. super-ionic conduction, oxidation, and reduction redox reactions below 600 ^{o}C [69]. This differs from single-phase materials, such as YSZ and SDC, where the high conductivity is realized by aliovalent doping to create oxygen vacancies inside the structure (bulk mechanism), which requires a high temperature to activate the ionic mobility.

Several kinds of electrode materials can be applied in the LTSOFC, for example LiNiO-SDC, NiO-SDC, and Ni-GDC (gallium-doped cerium) [70-71]. We chose the $Li_{0.15}Ni_{0.46}Cu_{0.15}Zn_{0.23}O$ (element content) as the electrode for the LTSOFC. LiNiO is often used as a cathode for the LTSOFC due to its high catalytic activity with O_2, and ZnO has a strong electronic conductivity after doping [72]. In addition, CuO easily reduces into an excellent electronic conductor, Cu, when combined with H_2 during operation.

The electrolyte layer must be dense to avoid any gas leakage and have poor electronic conductivity to avoid short-circuiting [73]. The electrolytes employed in the LTSOFC include gallium-doped cerium (GDC), carbonate-gallium-doped cerium (CGDC), SDC, NSDC (sodium carbonate-SDC) and CDC (calcium-doped

cerium) [74]. In this study, CSDC was used: the basic material was SDC with 15–35% carbonate salt to improve the ionic conductivity.

The ions in a CGDC- and CSDC-based LTSOFC are CO_3^{2-} and O^{2-}[25, 75, 62]. The ionic conductivity of CSDC has reached 0.4 s/cm (Fig. 2.5a) and the power density 1W/cm² at 470 °C and 1.7 W/cm² at 600 °C [25, 61], respectively. For comparison, the ionic conductivity of a traditional SOFC YSZ-electrolyte (Fig. 2.5b) is much lower than that of the LTSOFC electrolyte.

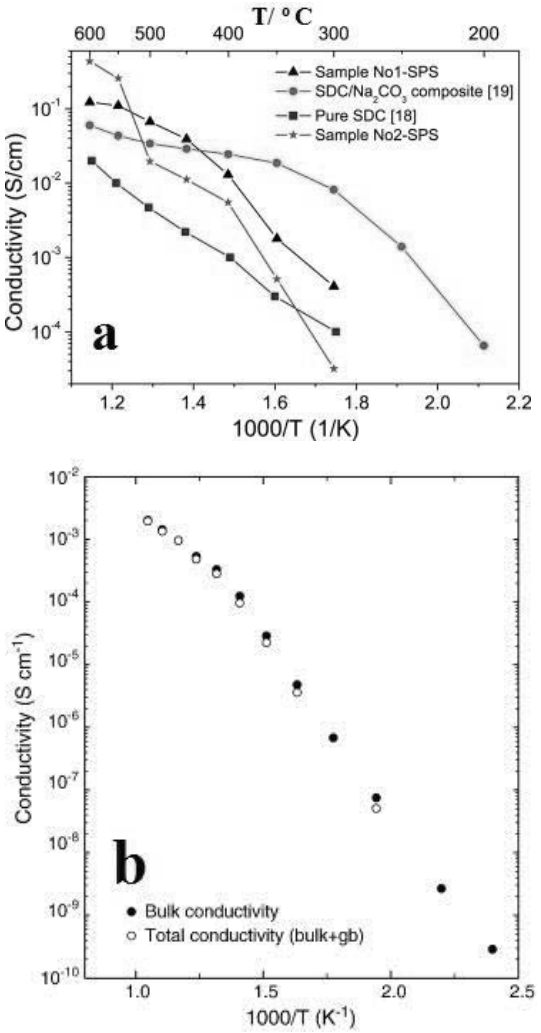

Figure 2.5. (a) Ionic conductivity of the LTSOFC electrolyte and (b) SOFC YSZ electrolyte [61, 77]. Reproduced with permission. Copyright 2014 Elsevier.

3. Experimental methods

The experiments with the nano-composite LTSOFC described in this study include the synthesis of electrolyte and electrode materials, fuel cell fabrication, fuel cell measurements, microscopy, and spectroscopy. This study employed three methods to synthesize the electrolyte material, two synthesis methods for the electrode materials, and two methods of fuel cell fabrication.

3.1 Materials synthesis

The co-precipitation method and freeze-drying method were applied to the electrolyte synthesis, and the solid mixing and slurry method for the electrode preparation, respectively.

3.1.1 Electrolyte prepared by co-precipitation (Publications III, IV)

Co-precipitation is the usual method for LTSOFC electrolyte preparation [77–79], as shown in Fig. 3.1.

Figure 3.1. Co-precipitation method.

$Ce(NO_3)\cdot 6H_2O$, $Sm(NO_3)\cdot 6H_2O$, Li_2CO_3, Na_2CO_3, and K_2CO_3 were used as the base materials. The synthesis proceeded as follows:

(1) Nitrate salts, $Ce(NO_3)\cdot 6H_2O$ and $Sm(NO_3)\cdot 6H_2O$, were dissolved in de-ionized water with continuous stirring with a magnetic stirrer;

(2) Then, alkali carbonate was dissolved into de-ionized water with the same stirring process as above. The molar quantity of the alkali carbonate is twice that of the $Ce(NO_3)\cdot 6H_2O$ and $Sm(NO_3)\cdot 6H_2O$;

(3) Solution number (2) was slowly added into solution (1) with vigorous stirring to avoid generating too high of a precipitation speed to form non-uniform white precipitation;

(4) The high speed stirring continued for 3 hours, then the liquid number (3) was washed 5 times with de-ionized water and filtered;

(5) The materials were dried after filtration for 24 hours, then sintered at 700 ^{o}C for 2 hours.

Step (5) produced a white powder, carbonated SDC, which was used as the electrolyte for the LTSOFC.

After this synthesis process, it became apparent that there is a defect in and advantage to this method. First, most of the alkali carbonate was consumed by the cerium nitrate and samarium nitrate, and the remaining alkali carbonate was lost in filtration or attached to the precipitation. This means the actual content of alkali carbonate is unknown. This will cause an electrolyte with low repeatability. There are also several defects in the method compared with the freeze-drying synthesis method.

It is a simple material synthesis method made available without any complicated devices, at a low cost, and in a short preparation time.

3.1.2 Electrolyte prepared by freeze drying (Publications II,V)

To improve the electrochemical performance, the freeze-drying method was applied with the steps shown in Fig. 3.2:

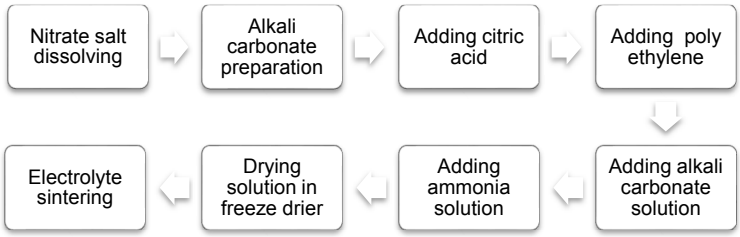

Figure 3.2. Freeze-drying process for electrolyte preparation.

The synthesis was as follows:

(1) Dissolve the $Ce(NO_3)\cdot 6H_2O$ and $Sm(NO_3)\cdot 6H_2O$ in de-ionized water with continuous stirring with a magnetic stirrer;

(2) Dissolve a suitable amount of alkali carbonate into de-ionized water with continuous stirring with a magnetic stirrer;

(3) Add a suitable amount of citric acid into the solution after step (1) to change the cerium ions and samarium ions into complex ions with continuous stirring;

(4) Add ammonia solution into the solution after step (3) until the pH reaches 10;

(5) Add the alkali carbonate solution into the solution in step (4) with continuous stirring;

(6) Dissolve a suitable amount of polyethylene into the solution after step (5);

(7) Freeze the solution from step (6), then dry it in a freeze dryer;

(8) Sinter the dry powders from step (7) at 700 ^{o}C for two hours after 36 hours of drying.

In step (3), a white deposit appeared in the beginning, and then disappeared when the ammonia solution was added into the solution continually.

Complex groups will deposit when the pH is less than 7 and dissolve when the pH is larger than 7. Then, the alkali carbonate solution will mix uniformly with the Ce^{3+} and Sm^{3+} in the solution after the alkali carbonate was added into the solution after step (4), and without any consumption with an alkaline solution. Then, the alkali carbonate will exist in an accurate content according to the calculation in the experiment.

The alkali carbonate and rare earth element ions were mixed more uniformly in a liquid state than that of the solid and liquid state mixing in the co-precipitation method. Compared with the co-precipitation method, the particle size of the electrolyte is readily controllable. Moreover, more interface boundary was generated in this method, resulting in increases in the ionic conductivity highway.

The SDC can be mixed with as much alkali carbonate as required, which can even reach 80%, but this is difficult with the co-precipitation method. The SDC used polyethylene to decrease the particle size of the electrolyte and to enable porosity in the electrolyte.

The freeze-drying method is more easily controlled, but the synthesis time is longer for it needs to be dried in a freeze drier and requires more equipment than that of the co-precipitation method, making it more complicated.

3.1.3 Electrolyte prepared by SPS (Publication I)

Spark plasma sintering (SPS) was also tested for the electrolyte preparation. Basically, it is a method to prepare the electrolyte layer out of the powder. It is a high-speed powder consolidation/ sintering technology for processing conductive and non-conductive materials. In SPS, a DC current generates heat internally. While traditional methods of materials processing often require hours to reach peak temperatures, SPS takes only a few minutes, i.e. it is very quick. The clear benefits of SPS are time and energy savings, and the ability to retain nano-

structures. The radiant heat also causes plastic deformation on the surface of the particles, which is necessary for high-density applications. The SPS presses the prepared electrolyte powder, e.g. by co-precipitation or freeze-drying into a high density, and the temperature of 600 °C is reached in several minutes [80–81].

3.1.4 Electrodes prepared by slurry method (Publications III, V）

The electrode of the LTSOFC was prepared by the slurry method, which enables a porous structure and high electrochemical performance in fuel cell measurement.

The method aims to prepare the electrode materials with a porous structure and high catalysis. The synthesis process is outlined below:

(1) Take an appropriate amount of chemical ($NiCO_3$, $ZnCO_3$, and $CuCO_3$) powder and put it in a beaker and mix the chemicals uniformly with de-ionized water;

(2) Add acid (citric acid or nitrate acid) to the mixture in step (1) to have a neutralization reaction with 33% of the mixture;

(3) Add 10% Li_2CO_3 by molar ratio of all the chemicals ($NiCO_3$, $ZnCO_3$, and $CuCO_3$) into the mixture in step (2);

(4) Keep stirring to make it mix uniformly and then dry the mixture;

(5) Sinter the powder mixture from step (4) at 700 °C for 2 hours and collect the resulting black powder (electrode material).

When the acid was added into the mixture in step (1), 33% of the carbonate changed into dissolvable nitrate salt and covered the surface of the carbonate particle when drying it. The nitrate has a lower point of decomposition compared to the carbonate in this experiment. Subsequently, the nitrate on the surface of the carbonate changed into an oxide shell first. With the temperature increasing,

the carbonate decomposed and released out CO_2; the oxide shell was broken, and the whole particle formed into ball-shaped porous structure.

In step (3), it is necessary to add the Li_2CO_3 after the neutralization reaction to avoid the lithium carbonate being consumed by the acid.

3.1.5 Electrodes prepared by solid mixing (Publications IV, V）

The solid mixing method of the electrode material is a simple method. Here, the ball mill is used as an alternative:

(1) Put a suitable amount of chemical ($NiCO_3$, $ZnCO_3$, $CuCO_3$, and Li_2CO_3) powder into the ball mill jars and mix with ethanol or water;

(2) Keep the ball mill running for 12 hours at a medium speed to mix the chemicals uniformly and decrease the particle size;

(3) Dry the slurry mixture from step (2), and then sinter the dry compound at 700 ^oC for 2 hours.

The ball mill time in step (2) is flexible according to requirements, 12 hours is sufficient to mix the chemicals uniformly, but the particle size of the chemicals becomes refined with longer processing time. Sometimes, the chemical was mixed in more simple devices like mortar without the ball mill.

The slurry method requires more devices, chemicals, and time compared with the solid mixing method.

3.2 Fuel cell fabrication

The electrode materials and electrolyte materials were applied in the LTSOFC after they were ready. Two kinds of fuel cell fabrication methods are described here.

3.2.1 Cold-pressing method (Publications I, II, III, V)

The cold-pressing method for LTSOFC fabrication is suitable to use for fast measurement of fuel cell. The electrode of the LTSOFC is a mixture of electrode material an electrolyte material to ensure the electrode of the fuel cell provides both ionic conductivity and electronic conductivity. The preparation process for the mixed electrode for the LTSOFC is detailed below:

(1) Mix the pure electrode material uniformly with the electrolyte material according to the volume ratio of 1:1;

(2) Mix a suitable amount of polyvinyl acetate solution uniformly with the powder;

(3) Dry the mixture from step (2), then grind it into powder;

The fuel cell fabrication equipment includes a 13 mm die with two 13 mm cylinders (the short one is used as the bottom cylinder and the longer one is used as the top cylinder), a CARVER 3851 hydraulic press, and an oven for sintering to strengthen the mechanical properties and remove the polymer in the electrode. The following details the fabrication process of the LTSOFC:

(1) Take a suitable amount of mixed electrode powder from the electrode preparation step (3) and put it into the fuel cell fabrication die (13 mm diameter). Press the powder into the die with the cylinder lightly to make it flat and smooth.

(2) Put a suitable amount of pure electrolyte materials on the first layer to make sure the second layer covers the entire first layer, and then press it like the previous step.

(3) Then, for the final layer, take a small amount of the mixed electrode, which is same as the first step, and make sure the second layer is totally covered by the third layer, then put the cylinder inside the die and press the cylinder at 100 MPa with the hydraulic press.

(4) Take the fuel cell out of the die and sinter the cell in the oven.

(5) Increase the sintering temperature step by step at a rate of less than one degree every 3 seconds. When the temperature reaches 600 ^{0}C, keep the temperature constant for 1 hour, then shut off the oven and keep the fuel cell in the oven until it reaches room temperature.

From the fuel cell fabrication process, it is worth noting that the fuel cell is a symmetrical structure with the same electrode material. It is reasonable to choose one thicker side electrode as the anode and a thinner side as the cathode. However, the most important consideration is that the electrolyte layer which must be thin and dense without leakage.

This is the traditional LTSOFC fabrication process, which was also applied in Publication III. In this study, the fabrication method was improved as it may cause a short circuit. The new method is described in Fig. 3.3:

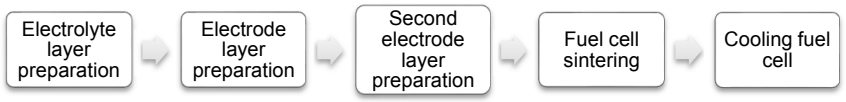

Figure 3.3. Cold-pressing process for fuel cell fabrication.

(1) Take a suitable amount of pure electrolyte powder, and put it into the fuel cell fabrication die (13 mm diameter). Press the electrolyte materials lightly in the die with the cylinder to make it flat and smooth;

(2) Put a suitable amount of mixed electrode powder from the electrode preparation step (3) materials on top of the first layer to make sure the second layer covers the entire first layer, and then press it like the previous step, then press the cylinder at 10 MPa with the hydraulic press;

(3) Take the bottom cylinder out carefully, and then put a small amount of the mixed electrode materials on the electrolyte layer. Make the new electrode layer flat, and put the bottom cylinder back. Then, press the two cylinders with 100 MPa with the hydraulic press;

(4) Take the fuel cell out of the die and sinter the cell in the oven and increase the temperature step by step at a rate of less than one degree every 3 seconds;

(5) When the temperature reaches 600 ^{o}C, keep the temperature constant for 1 hour, then shut off the oven and keep the fuel cell in the oven until it reaches room temperature.

The bottom cylinder should be thin enough to avoid a short circuit happening in the new fabrication method and ensure the edge of the fuel cell is also easy to clean.

The following operation is the fuel cell measurement after the LTSOFC was ready. It is not suitable to measure the fuel cell from the oven directly.

First, check the edge of the fuel cell to ensure that there is no electrode powder on it to avoid a short circuit. When the cell is ready without any short circuits, paint silver paste on the anode and cathode and let it dry. Make sure the silver paste is not painted on the edge of the fuel cell to avoid a new short circuit. The fuel cell is suitable to be measured after the silver painting is dry.

3.2.2 Hot-pressing method (Publication IV)

The cold-pressing method of fuel cell fabrication is easy to operate and requires only a short processing time. However, a cell with low mechanical properties and low yield for the short circuit may still happened. In addition, it is not easy to control the thickness of the fuel cell.

The low mechanical properties will cause a broken fuel cell if pressed too hard when measuring between the metal sample holders. However, if the sample holder is pressed too lightly, it can cause a gas leakage to happen.

In order to improve the fuel cell performance and resolve the problems mentioned above, the hot-pressing method was employed.

The hot-pressing method presses the anode, cathode, and electrolyte layers together in a hot state. Here, the electrode and electrolyte layers are membranes,

not powder. Then, the thickness is easy to control, and the electrolyte layer is denser than the cold-pressing methods.

The first process produces the electrode and electrolyte membrane, the fuel cell fabrication process operates when the membrane is ready in Fig. 3.4:

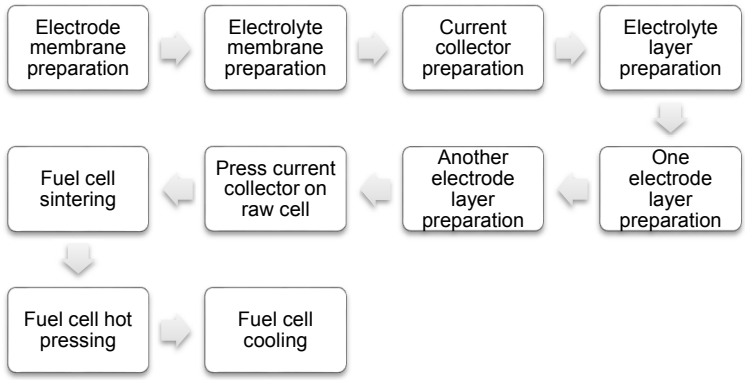

Figure 3.4. Cold-pressing process to fuel cell fabrication.

(1) Cut the electrode membrane into a round circle with a round tube knife;

(2) Then, cut the electrolyte membrane into a round circle with a round tube knife which is 1–2 mm larger than that used for the electrode cutting in order to avoid the anode and cathode membrane touching each other after pressing;

(3) Cut the silver network or copper network into a round shape, which is the same size as the electrode membrane;

(4) Put several layers of electrolyte together and lightly press it together, the layer number according to the membrane thickness;

(5) Choose two layers of electrode membrane after cutting and put in the middle of the pressed electrolyte layer and press lightly together;

(6) Then, reverse the pressed membrane after step (4) and put another layer of electrode in the middle of the electrolyte layer and repeat step (5);

(7) Choose one ready metal network and put it on the middle of the pressed membrane after step (6), then repeat step (5). Then, reverse the pressed compound after step (7), and put another layer of the metal network in the middle of the electrolyte layer and repeat step (5); the raw LTSOFC is now ready;

(8) Put the raw LTSOFC on one metal plate in the oven to sinter it at an increasing temperature rate of 1 degree per minute until it reaches 600 ^{o}C and keep sintering the cell for 1–2 hours;

(9) Take the metal plate and fuel cell out of the oven and press it immediately at 500 MPa or more with the hydraulic press;

(10) Take the fuel cell out when the temperature decreases to room temperature.

The sintering temperature is set at 600 ^{o}C to melt the alkali carbonate in the fuel cell and make it uniformly distributed in the cell. The binder in the fuel cell is totally combusted at this temperature. However, the sintering temperature is flexible according to different materials.

In order to strengthen the mechanical properties of the fuel cell, it is suitable to include another additive in the fuel cell, such as the ceramic fiber which can be mixed into the electrolyte layer to strengthen the cell. The metal network on the anode and cathode side is used as a current collector and also to strengthen the cell.

Now, the LTSOFC is ready by the hot-pressing method. Then, the silver paste is still necessary for the fuel cell measurement. The silver paste was painted on the current collector both on the anode side and cathode side, but less than the amount of silver paste painted on the cold-pressed fuel cell.

The hot-pressed membrane fuel cell has stronger mechanical properties and more stable electrochemical performance. However, it is more complicated and requires a longer preparation time as the electrode and electrolyte must be made into a membrane first.

3.3 Fuel cell measurements

To measure the electrochemical performance of the LTSOFC samples, a stainless steel fuel cell holder with a 13 mm external diameter and 9 mm inner diameter was employed as shown in Fig. 3.5.

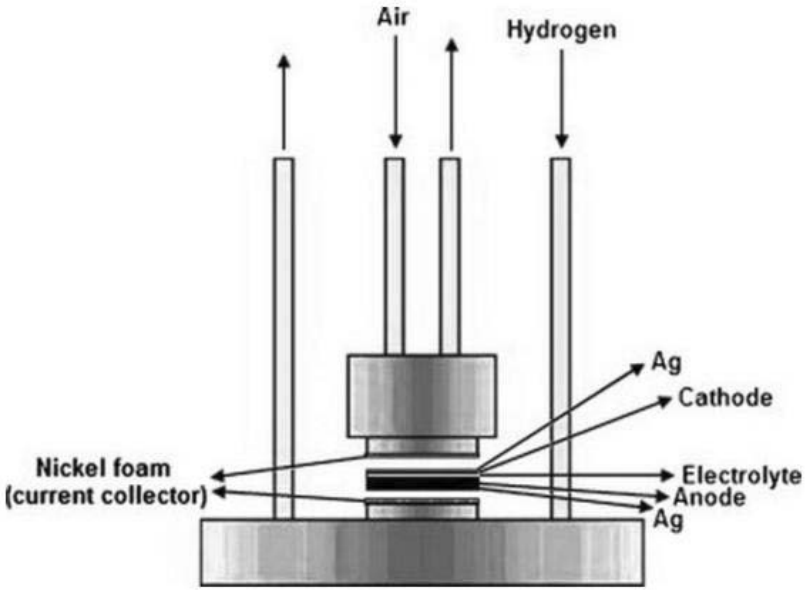

Figure 3.5. Schematic of the holder for the fuel cell measurements [98]. Reproduced with permission. Copyright 2007 Elsevier.

The fuel cell experiments included I-V, I-P, and the EIS measurements. These measurements also used the Scribner Associates 8900 CL measurement station and ZAHNER IM6 EIS as pictured in Fig. 3.6. In this fuel cell, H_2 was used as the fuel, and air, or a mixture of air and carbon dioxide, as the oxidant. Accordingly, a heating speed of 10 ^{o}C per minute was used to operate the fuel cell. Air was supplied to both sides of the electrolyte button cell in the impedance measurement using the 2-electrode alternating current (AC) method.

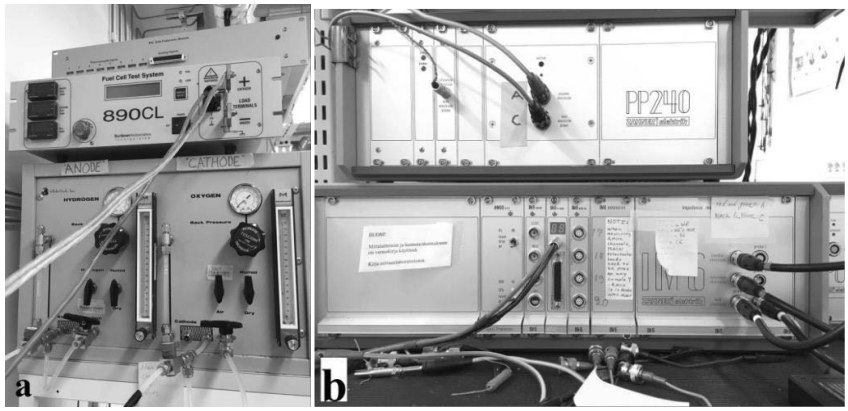

Figure 3.6. Experimental equipment: (a) fuel cell I-V measurement equipment, Scribner Associates 8900CL and (b) EIS measurement equipment, ZAHNER IM6.

An AC impedance spectroscopy was widely employed here on the solid electrolyte to obtain information on the charge transport behavior of both the bulk (grain interiors) and the grain boundaries of the cell [82]. Figure 3.7 illustrates a typical EIS spectrum and the equivalent circuit for the sample. The semi-circle at high frequency represents the bulk properties, the intermediate frequency represents the grain boundary, and the low frequency semi-circle represents the electrode contribution. The separate semi-circles are formed due to the differences in the relaxation time of the oxygen ion transfer through the grain, grain boundary, and electrode [83]. Various combinations of electrical elements, such as resistances, capacitances, and inductances, describing the different electrical phenomena are used to fit the experimental data to an equivalent circuit model [83].

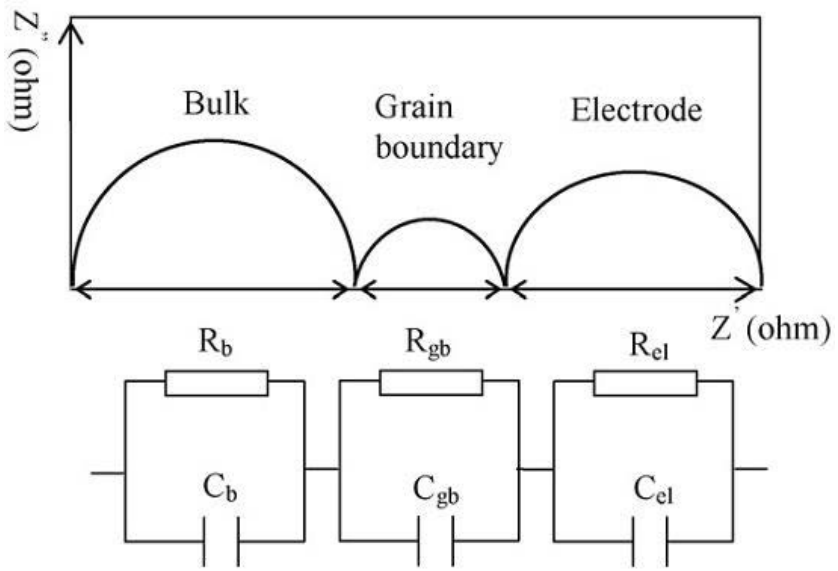

Figure 3.7. Illustration of a typical impedance plot for a polycrystalline sample with equivalent circuits [82]. Reproduced with permission. Copyright 2007 Elsevier.

For a sample with a thickness of L and a cross section area of A, the bulk conductivity, σ_b, and the grain boundary conductivity, σ_{gb}, can be expressed as $\sigma_b = LA^{-1}R_b^{-1}$ and $\sigma_{gb} = LA^{-1}R_{gb}^{-1}$, where R_b and R_{gb} are the bulk and grain boundary resistances, respectively. The total conductivity, σ_T, is then given by $1/\sigma_T = 1/\sigma_b + 1/\sigma_{gb}$ [82].

3.4 Microstructural analyses

The microstructural analyses in this study included SEM (EDS and mapping), TEM, XRD, and XPS. For the SEM and EDS device, a JSM-7500F was used. The TEM is a JEOL 2200FS (200 kV) and the XRD is a PANalytical X'Pert PRO MPD Alpha-1. All of these were available in the Nano-Microscopy Center at the Department of Applied Physics at Aalto University. The SPS equipment used for plasma sintering belonged to the Department of Material Science and Engineering of Aalto University.

4. Main results

In this chapter, the results for the following components are described:

- LiNiCuZn electrode
- CSDC electrolyte
- Nano-composite LTSOFC

The results of the microstructure and electrochemical characterization are presented.

4.1 LiNiCuZn electrode (Publications III, IV, V)

For the electrode preparation, we employed the solid mixing and slurry methods explained earlier in Chapter 3. Figure 4.1 shows the SEM images from the electrodes prepared with these two methods. The size of the particles by the slurry method was clearly smaller than with the solid mixing leading to a lower polarization resistance to be shown later. Therefore, the main focus was put on the slurry method.

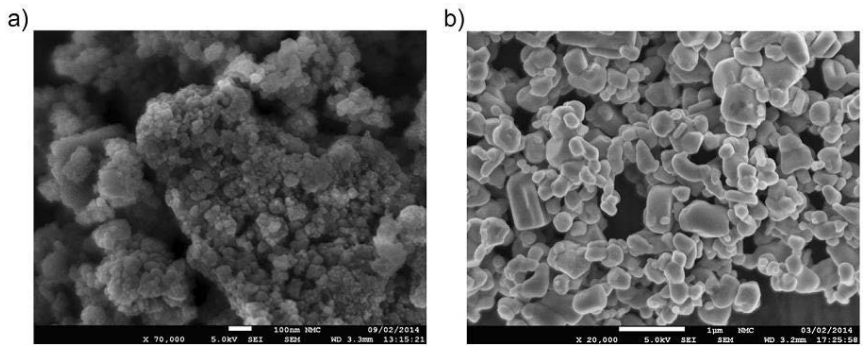

Figure 4.1. SEM images of electrode samples with a) slurry and b) solid mixing methods. Reproduced with permission from Publication V. Copyright 2016 Elsevier.

The LiNiCuZn oxides synthesized by the slurry method are shown in Fig. 4.2. The SEM characterization reveals that the material particles form clusters of quite regular circular shapes of 800–1000 nm in size. The TEM analysis illustrates that the crystal size of the particles is about 30 nm with a regular shape. In this regard, it could be expected that small particle sizes lead to a large effective surface area improving electrochemical performance.

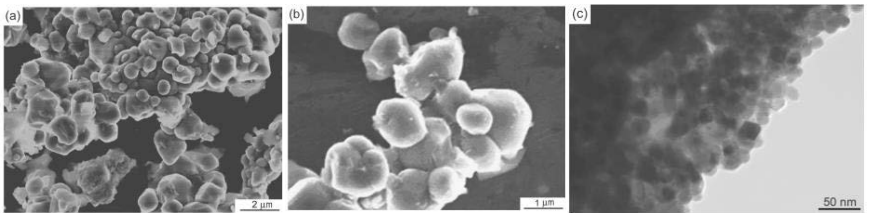

Figure 4.2. FESEM (a,b) and TEM (c) images of the LiNiCuZn oxide. Reproduced with permission from Publication III. Copyright 2012 ASP.

The XRD patterns of the compound are illustrated in Fig. 4.3, identifying the CuO, ZnO, and $Li_{0.28}Ni_{0.72}O$.

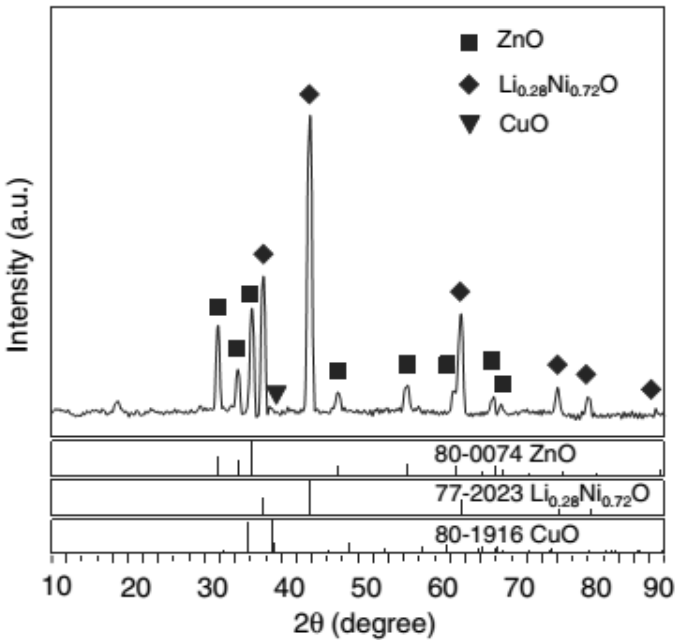

Figure 4.3. XRD pattern of the LiNiCuZn oxides. Reproduced with permission from Publication IV. Copyright 2017 OneCentralPress.

An electrode cell with a thickness of 1 mm and a diameter of 13 mm was made from a mixture of electrode and electrolyte powders to measure the EIS. In the experiment, the same gas (H_2 or air) was supplied to both the anode and cathode sides of the electrode pallet. The temperature variation was less than 3 ^oC during the measurements. Figure 4.4 shows the electrochemical resistance of the mixed electrode. The half semicircle at high frequency comes from the ionic reaction between the electrolyte and electrode, and the semicircle at the low frequency is caused by gas diffusion or absorption from the electrochemical kinetics in the electrode.

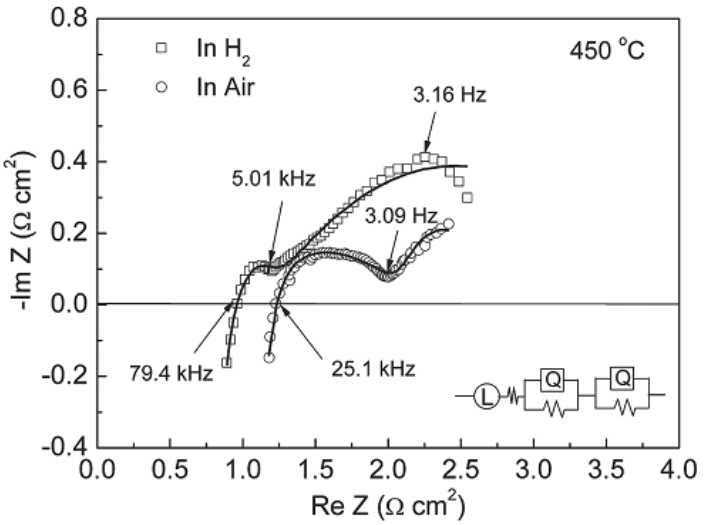

Figure 4.4. Electrochemical impedance spectrum of a LiNiCuZn-oxide electrode for LTSOFC, both in dry H_2 and air at 450 °C [84]. Reproduced with permission from Publication III. Copyright 2012 ASP.

The total resistance is 0.77 Ω/cm² and 0.87 Ω/cm² of the electrode reaction in H_2 and air separately, and a charge transfer resistance of 0.38 Ω/cm² and 1.3 Ω/cm² in H_2 and air in Fig. 4.4, respectively. The lower reaction kinetic of the electrode in H_2 demonstrated that the fuel cell anode has lower resistance in the fuel cell reaction; thus, the fuel cell polarization is dominated by the cathode. So it is necessary to improve the conductivity of the cathode to improve the electrochemical performance of the fuel cell, e.g. to reduce the cathode thickness.

The resistance of the LiNiCuZn electrode is less than that of the resistance of a conventional $La_{0.75}Sr_{0.2}BO_{3-6}$ (B= Mn, Fe) cathode for the SOFC operated in oxygen at 800 °C. The polarization resistance of the anode was lower than that of the $Ce_{1-x}Fe_xO_{2-6}$ (x=0.1, 0.2) anode in dry hydrogen at 550 °C [85]. The electrochemical performance of the fuel cell was enhanced by the outstanding conductivity of the LiNiCuZn enhances (see Fig. 4.17).

The EIS results are shown in Fig. 4.5 [86]. The polarization resistance of the LiNiCuZn electrode by the slurry method was 0.21 Ω/cm² at 550 °C, which was less than the 0.31 Ω/cm² by the solid mixing method. This may have been one of

the main reasons for the lower fuel cell performance in later experiments in Publication IV.

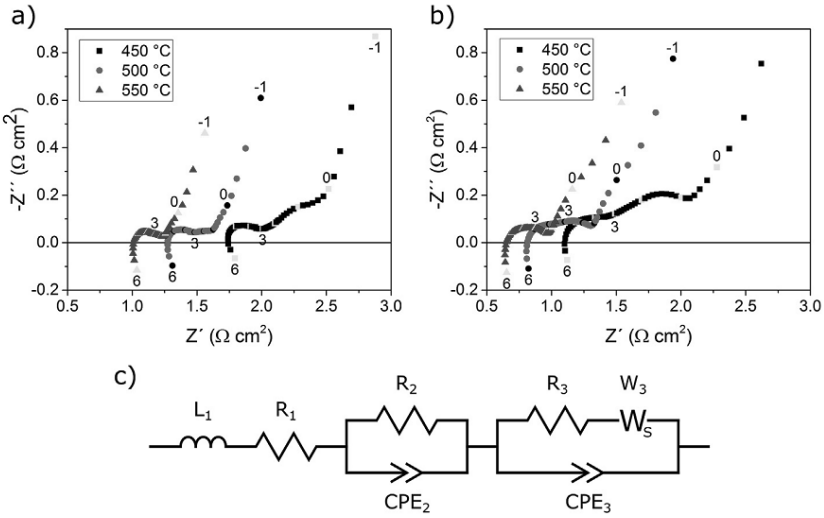

Figure 4.5. The electrochemical impedance spectra of symmetric fuel cells prepared by a) the slurry and b) the conventional solid mixing preparation methods. Measurements were conducted in air at 450 °C, 500 °C, and 550 °C. The equivalent circuit used for modeling the impedance data is also shown. Reproduced with permission from Publication V. Copyright 2016 Elsevier..

4.2 CSDC electrolyte (Publications I, II, IV)

4.2.1 Co-precipitation method (Publication IV)

The CSDC electrolyte powders from the co-precipitation synthesis phase were analyzed with SEM and TEM in Fig. 4.6 to understand the morphology and structure of the powder. Two samples were investigated:

Sample 1: CSDC ($Ce_{0.8}Sm_{0.2}O_{1.9}$) powder was prepared by co-precipitation.

Sample 2: 10 g of Sample 1 was washed and filtrated 5 times with 5 liters of de-ionized water and finally dried in the oven at 200 °C.

The microstructure of the two samples is shown in Figure 4.6; Sample 1 is in the right column and Sample 2 in the left one. Figure 4.6 (a,b) shows the morphology and particle shapes, (c, d) the shape and size of the crystals, and (e,f) the single crystals and their phases.

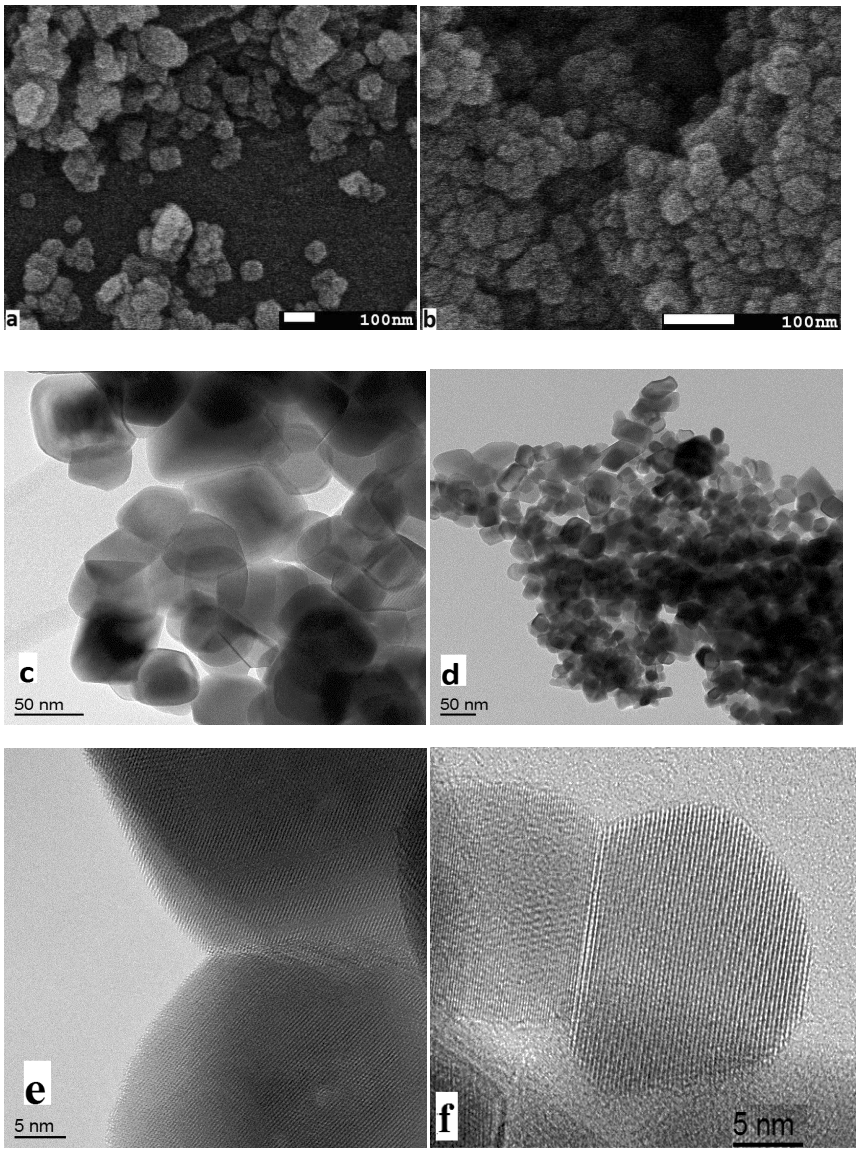

Figure 4.6. Morphological analyses of two samples. (a) SEM Sample 2, (b) SEM Sample 1, (c, e) TEM Sample 2, and (d, f) TEM Sample 1. Reproduced with permission from Publication IV. Copyright 2017 OneCentralPress.

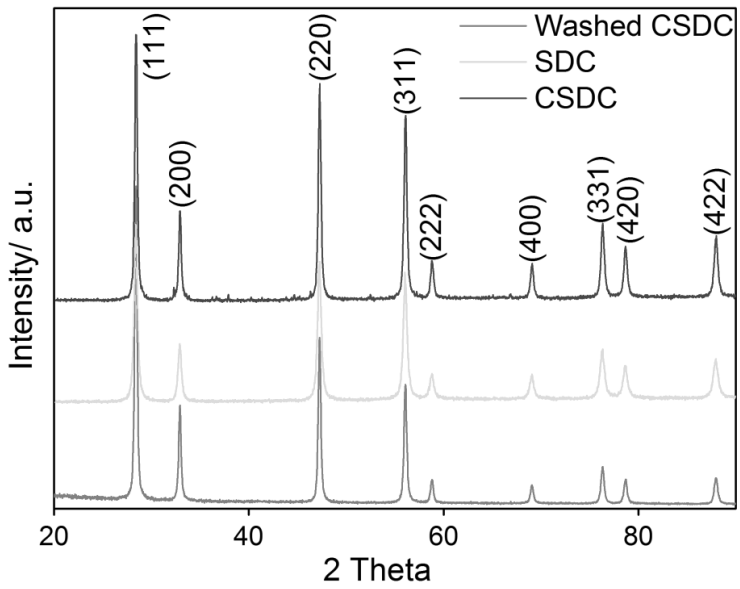

Figure 4.7. XRD spectra of the samples 1, 2, and SDC. Reproduced with permission from Publication IV. Copyright 2017 OneCentralPress.

Samples 1 and 2 have almost the same particle shape, and the agglomerate sizes are around 100–200 nm. The crystal sizes of Sample 1 and 2 are around 50–100 nm, which is less than their particle size. The crystal has clearly one phase only indicating that the carbonate has not penetrated inside the crystal as that would lead to extra phases, also verified by the XRD diffraction in Fig. 4.7. This indicates that the alkali carbonates exist not in a crystal state in the SDC, but they would be in an amorphous state, or alternatively, the alkali and carbonate elements are not combined to form the alkali carbonate.

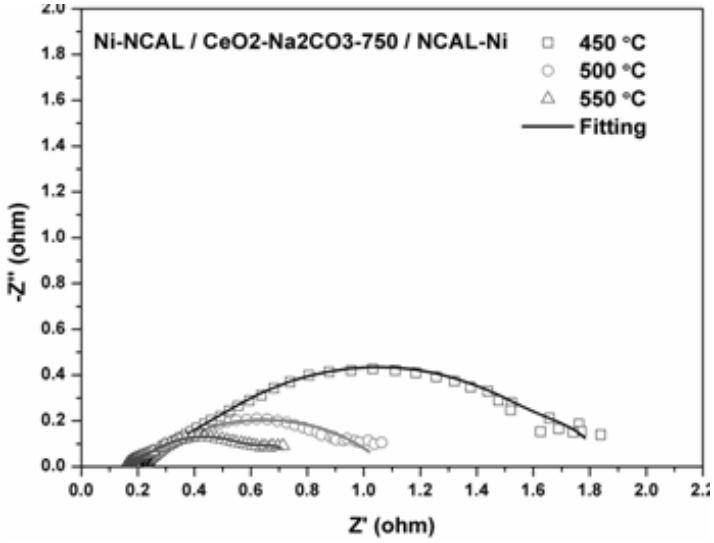

Temp.°C	R_0	R_1	R_2	R_3
450	0.226	0.464	1.274	0.199
500	0.182	0.230	0.872	0.170
550	0.158	0.053	0.419	0.158

Figure 4.8. EIS measurement of a test cell (Ø13mm) with an electrolyte made by co-precipitation using symmetrical electrodes. R_0 = ohmic resistance; R_1 = bulk resistance of oxygen ionic transfer in electrolyte; R_2 = grain boundary resistance of the electrolyte; R_3 = oxygen molecule adsorption and dissociation resistance, or the non-charge transfer resistance. $R_{total} = R_0+R_1+R_2$.

In Fig. 4.8, we show the EIS of a test pellet made from the electrolyte powder by the cold-pressing method followed by gentle sintering for 1.5 hours at 550 °C. The pellet is 1.3 mm thick, so the $\sigma = L/RA' = 0.13cm/(0.6297\Omega \times 1.3267cm^2) = 0.155$ S/cm.

4.2.2 Freeze-drying method (Publication II)

Three different electrolyte samples with different element contents were prepared and analyzed, as shown in Table 4.1.

Table 4.1. Alkali contents of sample No.1, 2, and 3.

Content (%) / Name	Li_2CO_3	Na_2CO_3	K_2CO_3	SDC
No. 1	7	11.5	11.5	70
No. 2	15	7.5	7.5	70
No. 3	6	12	12	68

First, an EDS analysis was made of the samples in Fig. 4.9 showing the Ce, Sm, K, Na, O, and C elements in the samples, but lacking Li which is hard to detect by EDS. The XRD in Fig. 4.10 shows only the peaks from the SDC crystals. Within θ = 20-48°, there are several smaller peaks which are linked to $LiNaCO_3$ and K_2CO_3, but compared to the 30% and 38% alkali carbonate contents in Samples 1, 2, and 3, these peaks are too weak. Figure 4.9 and 4.10 imply that most of the alkali carbonate seems to exist in an amorphous state in CSDC [87].

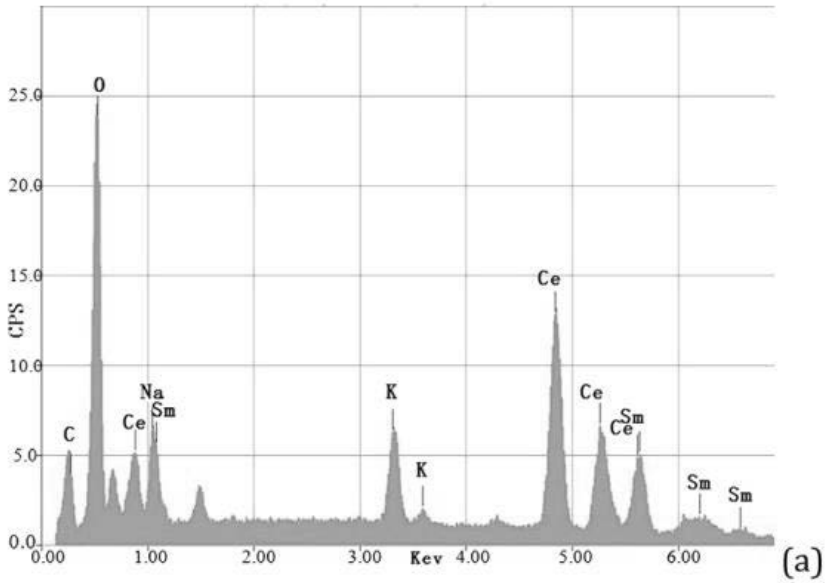
O
C
Na
Ce
Sm
K
Ce
Ce
Sm
Ce
Sm
Sm
K
CPS
25.0
20.0
15.0
10.0
5.0
0.0
0.00
1.00
2.00
3.00
Kev
4.00
5.00
6.00

(a)

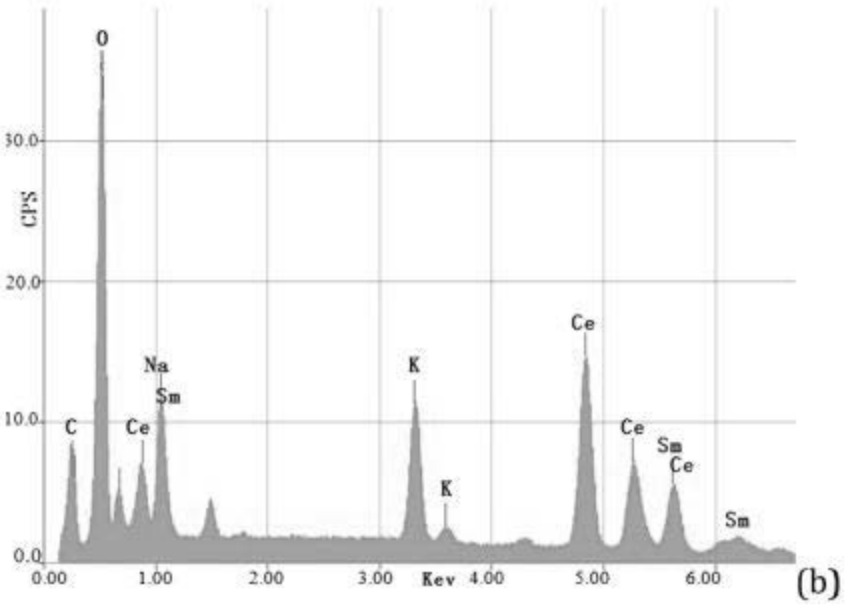
O
C
Na
Ce
Sm
K
K
Ce
Ce
Sm
Ce
Sm
CPS
30.0
20.0
10.0
0.0
0.00
1.00
2.00
3.00
Kev
4.00
5.00
6.00

(b)

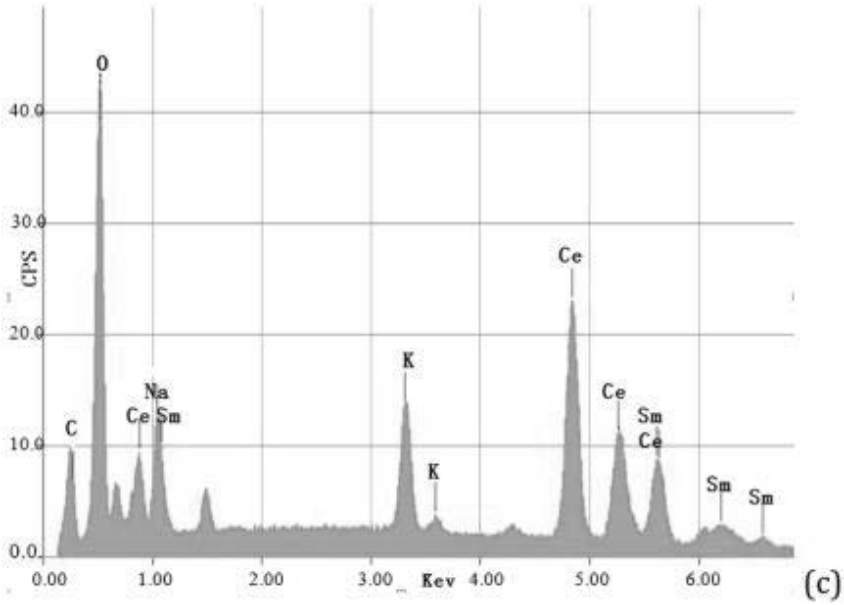

Figure 4.9. EDS analysis of the electrolyte samples, (a) Electrolyte No. 1, (b) Electrolyte No. 2, and (c) Electrolyte No. 3. Reproduced with permission from Publication II. Copyright 2013 Elsevier.

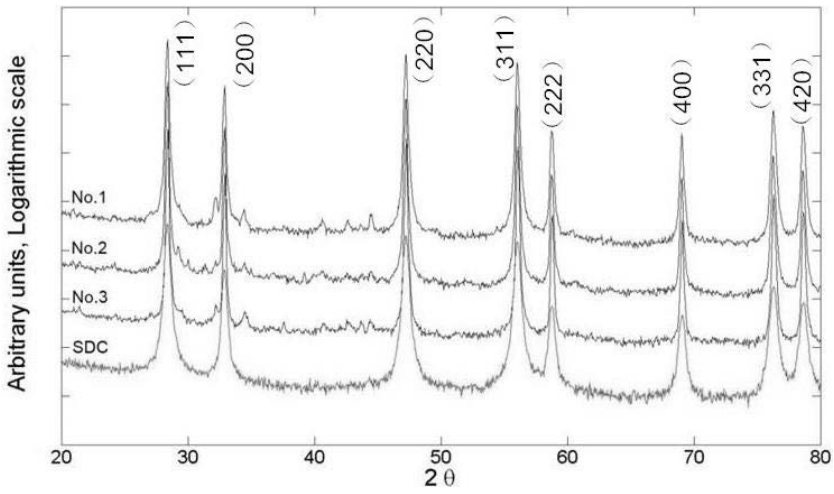

Figure 4.10. XRD spectra of the samples. Reproduced with permission from Publication II. Copyright 2013 Elsevier.

The micro structural analysis with SEM in Fig. 4.11 shows that all samples exhibited about the same type of irregularly shaped 100–200 nm circular particles.

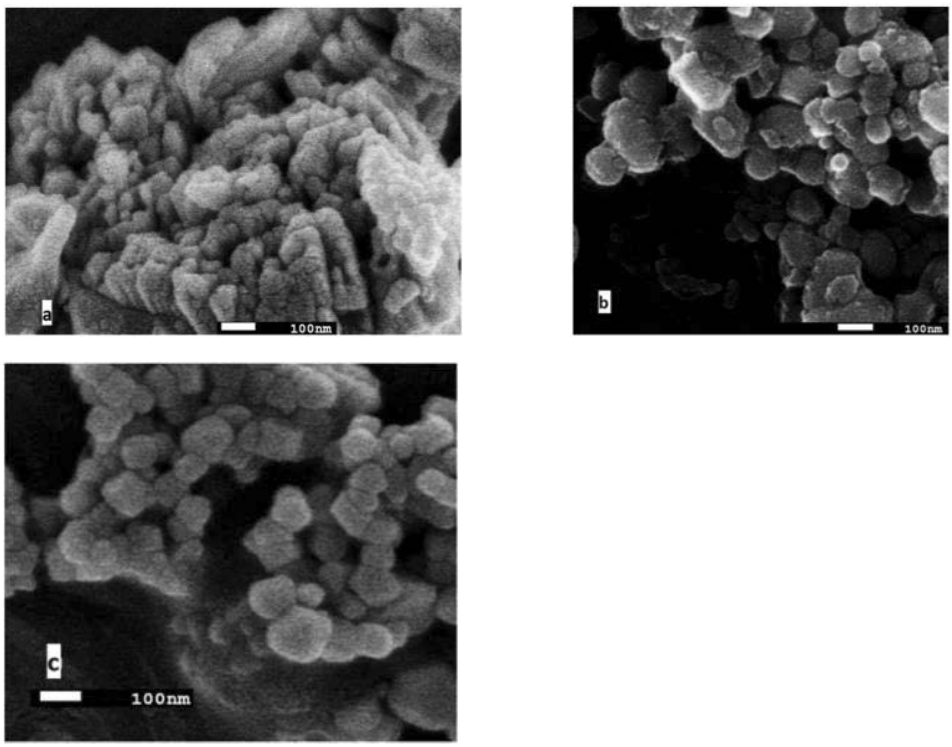

Figure 4.11. SEM images of electrolyte samples: a: No. 1, b: No. 2, and c: No. 3. Reproduced with permission from Publication II. Copyright 2013 Elsevier.

For Sample 2, an EDS element mapping was conducted in Fig. 4.12, which illustrates similar distributions of carbon, oxygen, sodium, and potassium indicating that these four elements compose chemicals together. However, cerium and samarium have different distributions compared to the above elements. This could indicate that Li_2CO_3, Na_2CO_3, and K_2CO_3 exist in the electrolyte. Combining the EDS element distribution and the XRD diffraction patterns provides evidence that the alkali carbonate in the SDC is in an amorphous state.

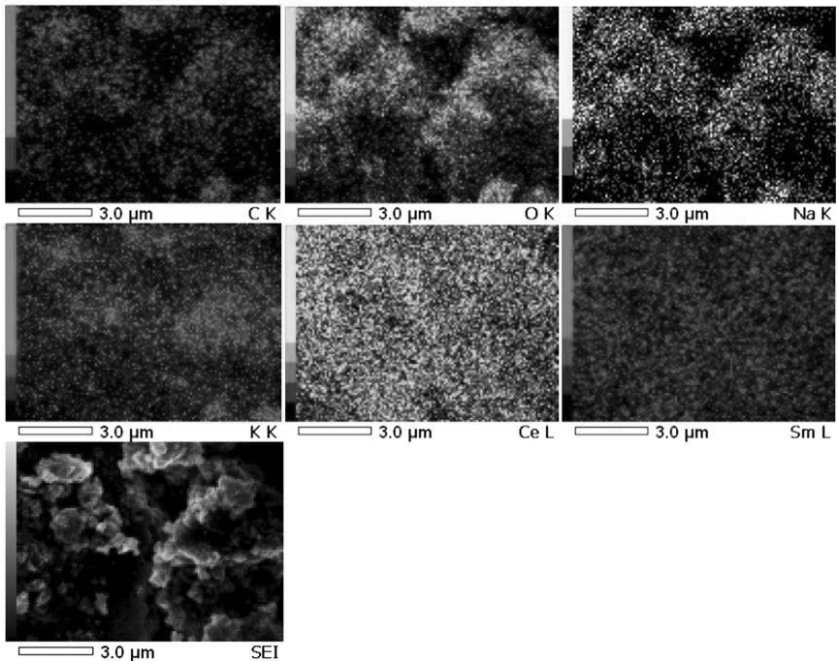

Figure 4.12. EDS element mapping of electrolyte Sample 2. Reproduced with permission from Publication II. Copyright 2013 Elsevier.

Finally, the electrochemical parameters were determined for the electrolyte sample. A 1 mm thick and 13mm in diameter electrolyte cell/pellet was pressed from a nano-composite $LiNaKCO_3$-SDC electrolyte with symmetric silver paint on both sides. The measurements were conducted in air with less than 3 ^{o}C temperature variations during the measurements. Figure 4.13 illustrates the measured ionic conductivities of the Samples.

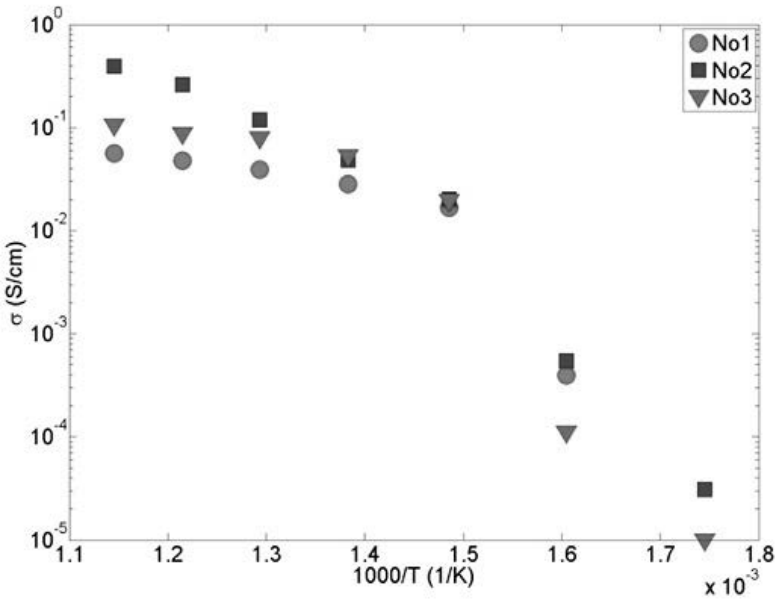

Figure 4.13. Ionic conductivity versus temperature (1/T) of the electrolyte samples. Reproduced with permission from Publication II. Copyright 2013 Elsevier.

Sample No. 2 has the highest ionic conductivity compared to the other two samples. The ionic conductivity of all samples increases rapidly in the interval 350–400 °C. All samples exhibit a similar shape between the conductivity and 1/T due to a softening of the alkali carbonate [64, 88]. At around 500 °C, the LiNa-carbonate-doped ceria composite synthesized by the co-precipitation method demonstrates a rapid conductivity jump in the soft area [87, 89, 90]. The change of softening temperature may be caused by the mixing size and mixing state. The highest conductivity of Sample No. 2 reached a value of 400 mS/cm at 600 °C. Sample No. 2 has the same alkali content as Sample No. 1, but a better ionic conductivity due to its higher lithium content. Sample No. 3 has the highest alkali carbonate content of all the samples, and it needs more energy to soften leaving its conductivity lower at T < 400 °C.

Sample 1 was analyzed in more detail in Fig. 4.14. There is just one semicircle in the high frequency area and one tail at low frequencies compared to the three typical semicircles in Fig. 3.7 [91–93]. The only semicircle in the LTSOFC

electrolyte represents the ionic resistance caused by the ionic conductivity with combined grain boundary and bulk resistance. The tails are caused by gas and ion diffusion in the electrode which was painted on the top of the electrolyte pellet.

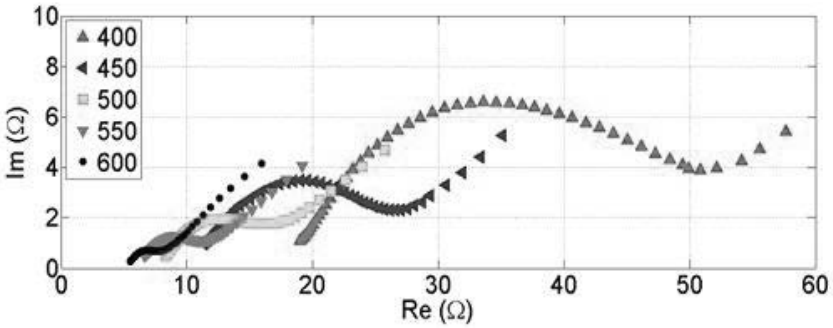

Figure 4.14. Impedance spectrum of electrolyte Sample No. 1. Reproduced with permission from Publication II. Copyright 2013 Elsevier.

In conclusion, it is possible to state that the ionic conductivity of the electrolyte and the interfacial area between the SDC and carbonate were clearly improved by the freeze-drying synthesis method.

4.2.3 Spark plasma sintering (Publication I)

Two sample electrolytes by the Spark Plasma Sintering (SPS) method were analyzed in detail. The element contents of sample electrolyte No.1 and No.2 are shown in Table 4.2.

Samples No. 1 and 2 processed by SPS and for comparison with the normal method (the electrolyte pellet was made from electrolyte powder by cold pressing, followed by a gentle sintering for 1.5 hours at 550 ^{o}C) were characterized by SEM in Fig. 4.15. A particle size of 30–50 nm with a regular shape and similar particle size distribution is clearly observed. Comparing the morphology of Sample No. 1, which is processed by the normal press method, and Sample No. 2, with the SPS method in Fig. 4.14a and c, shows that the SPS sample exhibits a distinctly densified structure compared to the normal pressed sample which has a slightly loosely-packed layout with clear pores distributed among the particles. The same

is seen in Fig. 4.15 b and d, which demonstrates the enhanced density of the electrolyte cell from the SPS while maintaining the same particle size albeit with quick heating and a short processing period in SPS. The well-packed particle structure with fewer pores, thinner structure, and more comprehensive interface system should enhance the ionic conductivity of the electrolyte.

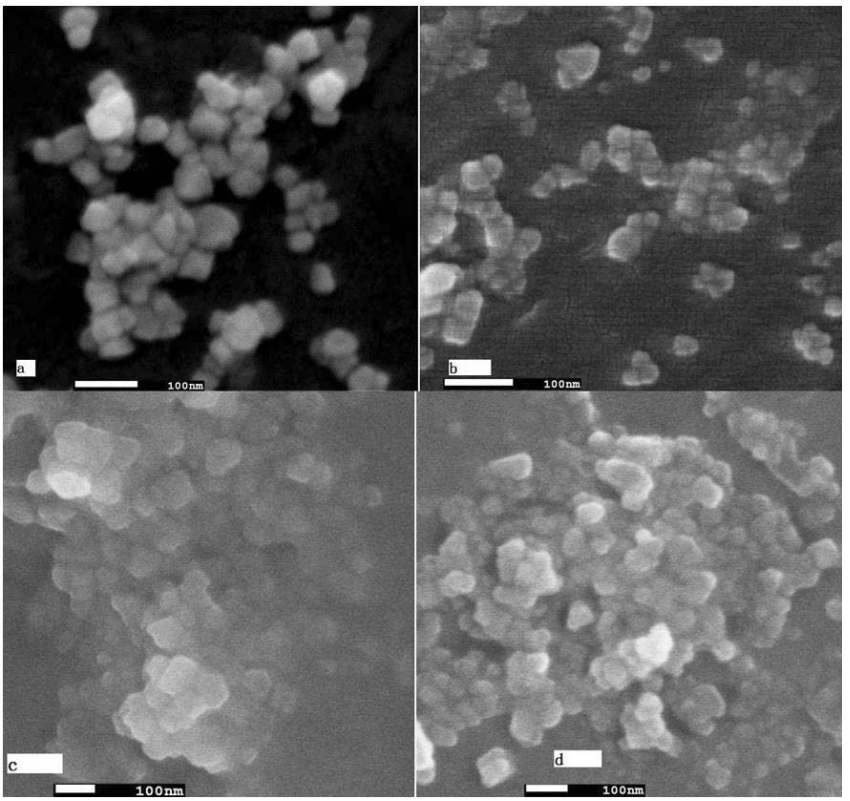

Figure 4.15. SEM of No. 1 and No. 2 electrolytes fabricated by the normal method (cold pressing + gentle sintering) (a, b) and spark plasma sintering (c, d). Reproduced with permission from Publication I. Copyright 2014 Elsevier.

The XRD spectra of pure SDC and electrolyte Samples 1 and 2 in Fig. 4.16 demonstrate similar shapes with peaks originating from SDC, which also confirm that the alkali carbonate exists in an amorphous state [94].

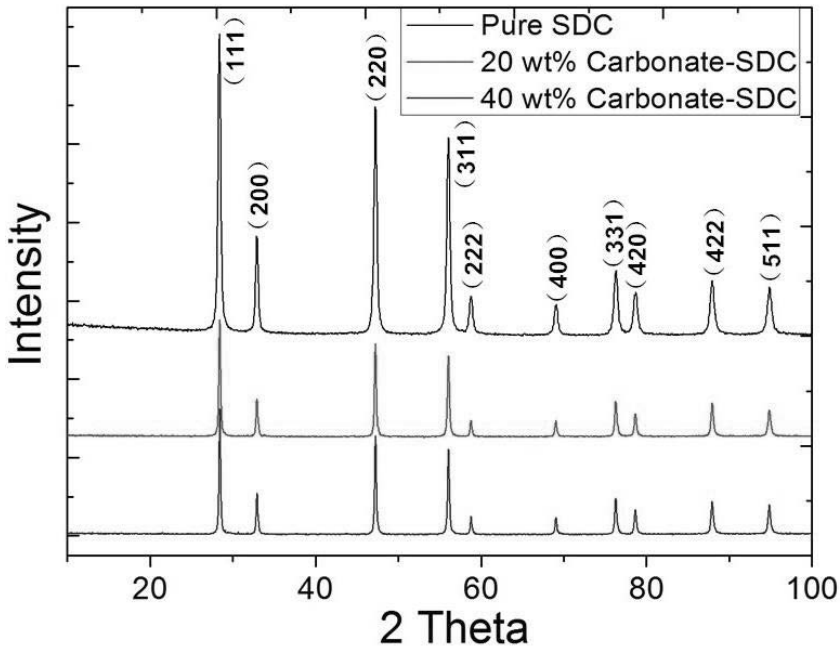

Figure 4.16. XRD spectra of Samples No.1, Sample No.2, and pure SDC. Reproduced with permission from Publication I. Copyright 2014 Elsevier.

To measure the electrochemical performance, the electrolyte powder was put into a pellet/cell form. The two electrolyte samples were pressed by SPS into a high density electrolyte pellet/cell; for comparison, cells were also prepared with the normal method (cold pressing + sintering). Then, the EIS and the ionic conductivity of the cells were measured in air atmosphere.

The EIS measurement of electrolyte Sample No. 1 and 2 is shown in Fig. 4.17.

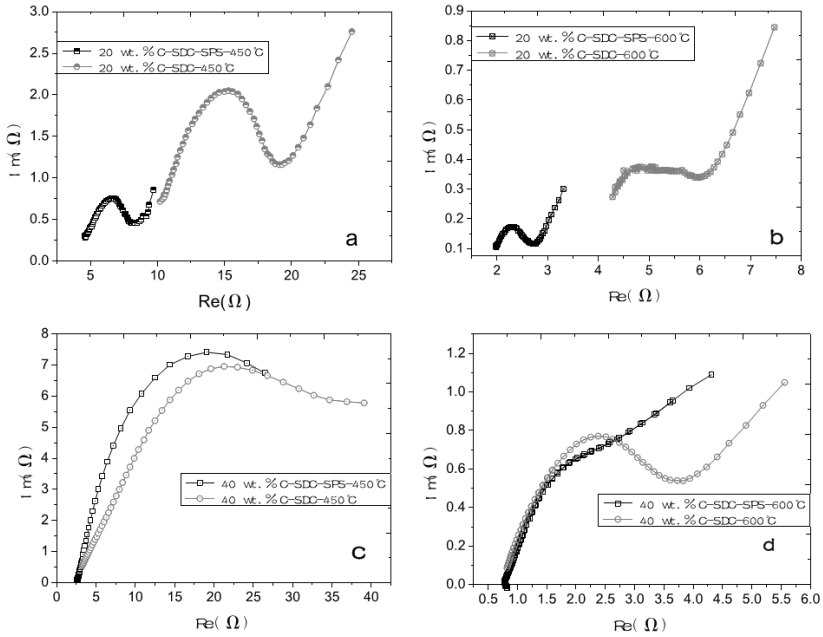

Figure 4.17. Impedance spectra comparison of electrolyte No. 1 and No. 2 processed by the normal way (cold pressing + gentle sintering) and SPS at 450 ºC and 600 ºC (a: 450 ºC 20 wt. %. Carbonate-SDC; b: 600 ºC 20 wt. % Carbonate-SDC; c: 450 ºC 40 wt. % Carbonate-SDC; and d: 600 ºC 40 wt. % Carbonate-SDC). Reproduced with permission from Publication I. Copyright 2014 Elsevier.

The EIS measurement results are almost the same in Fig. 4.17 (c) at 450 ºC, both the SPS sample and the normal pressed sample cell have one incomplete semicircle which is caused by grain boundary resistance combined with the bulk resistance [95]. When the operating temperature increased to 600 ºC in Fig. 4.17 (d), the SPS electrolyte cell has only one curving tail instead of one semicircle attribute to the electrode contribution, but the normal pressed electrolyte sample still has one incomplete semicircle. In the EIS of the SOFC, the tail represents the redox speed or diffusion mechanisms on the electrodes [96-97]. The resistance of the SPS in Fig. 4.17d was dominated by the resistance of gas and ion diffusion in the electrode, not electrolyte.

Similarly, one semicircle with a tail or just a single tail/partial semicircle is quite commonly found from the literature for the composite electrolyte at high temperatures [93, 97], for the grain boundary semicircle vanished when the

carbonate is melting. Furthermore, it can be noticed that the SPS samples show smaller resistance compared to the samples processed by the normal method at 450 °C and 600 °C. Therefore, it is clearly demonstrated that SPS processing enhanced the ionic conductivity of the SDC-carbonate nano-composite electrolyte.

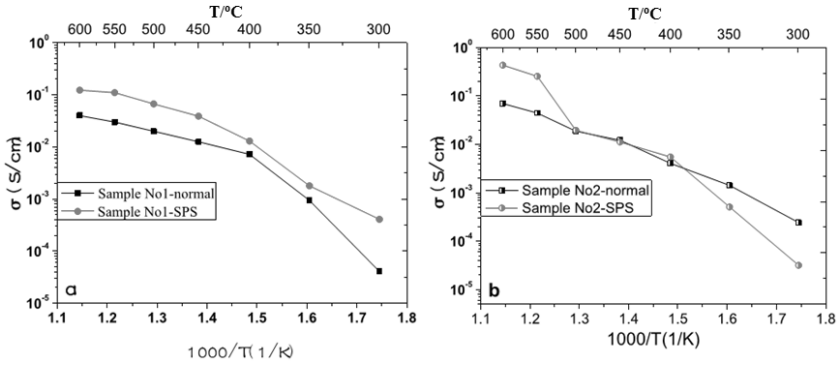

Figure 4.18. Comparison of temperature-dependent conductivity curves of Sample No. 1 (a) and No. 2 (b) processed by SPS and normal processing (cold pressing + sintering). Reproduced with permission from Publication I. Copyright 2014 Elsevier.

In Fig. 4.18, when the alkali carbonate content is 40%, the SPS pellet has an ionic conductivity 4.3 x 10^{-1} S/cm at 600 °C which is notable higher than that of the normal processed sample. The conductivity of the SPS Sample No. 2 was lower than that of the normal processed Sample No. 2 during 300–400 °C. From the XRD spectra, there are small peaks besides the SDC peaks which indicate that an alkali carbonate crystal exists in Sample No. 2. It requires more thermal energy to soften the crystal to integrate the interface among the SDC particles. But when the operating temperature rose above 500 °C, the outstanding ionic conductivity enhancement of Sample No.2 was displayed; the ionic conductivity was enhanced five times compared to the normal processed electrolyte pellet. In Fig. 4.17c, the Sample No.1, the SPS electrolyte pellet always exhibits higher ionic conductivity compared to the normal processed electrolyte pellet.

Fig. 2.5 showed the conductivity results of the No. 1 and No. 2 electrolyte processed by the SPS technique in the present work as compared to that of the pure SDC electrolyte [99] and the SDC/Na_2CO_3 nano-composite reported in the literature [100]. It can be seen that the conductivity of both composite electrolytes

are of several times higher magnitude than that of pure SDC in the temperature range of 300–600 ^{o}C. The significantly enhanced ionic conductivity of these composite electrolytes demonstrates a distinct “nano-composite effect”, which can be ascribed to the interfacial interaction. Besides, the No. 1 SDC carbonate composite cell fabricated by SPS exhibits even higher conductivity than the state-of-the-art SDC/Na_2CO_3 nano-composite at a temperature above 450 ^{o}C and the similar superior conductivity enhancement of No. 2 happened at about 500 ^{o}C. Therefore, it is confirmed that using the SPS technique can further improve the ionic conductivity of the composite electrolyte by increasing material densification. However, the SPS-made layer were mechanically very fragile, and full scale fuel-cells could not yet be manufactured with this method.

4.3 Performance of nano-composite LTSOFC (Publications III, IV)

4.3.1 LiNiCuZn electrode and CSDC electrolyte (Publication III)

The most important property of a fuel cell is the electrochemical performance, especially the power density. The power density of the fuel cell is not only affected by fuel cell ionic and electronic conductivity, but it is also affected by the fuel cell fabrication, structure, temperature, fuel, and oxidant.

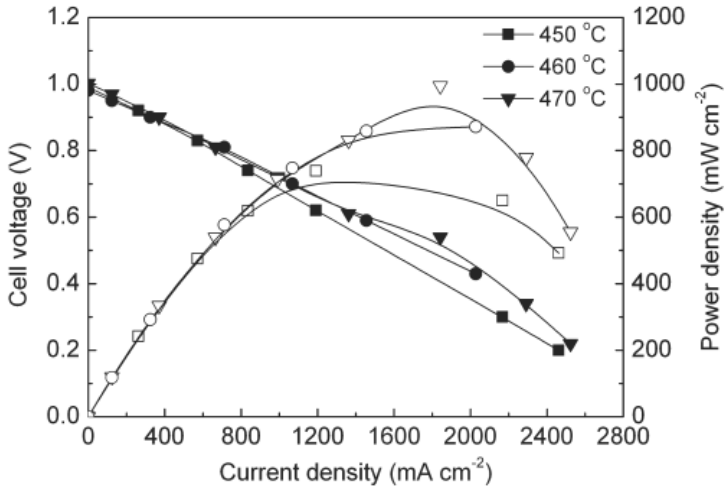

Figure 4.19. The electrochemical performance of the compound LTSOFC mixed with LiNiCuZn oxides made by the slurry method as an electrode. The electrolyte was prepared by co-precipitation. Reproduced with permission from Publication III. Copyright 2012 ASP.

In this study, the LTSOFC is a button cell with a 13 mm diameter which is made from electrode and electrolyte powder, the inner diameter of the fuel cell sample holder is 9 mm. The LTSOFC has a symmetric electrode and anode support structure. With LiNiCuZn oxide (LiNiCuZn oxide mixed with half volume NSDC) as the electrode and CSDC electrolyte which is synthesized by the co-precipitation method, the LTSOFC displays an outstanding power density of 1000 mW/cm^2 at 470 ^{o}C in Fig. 4.19.

Table 4.1. Comparison of the cell performance of the LTSOFCs reported before and in the present work.

Anode	Cathode	Electrolyte	Test temperature (°C)	Maximum power density (mW cm^{-2})	Reference
Ni-SDC	$Ba_{1-x}Pr_xCo_{1-y}Fe_yO_{3-\delta}$	SDC	650	860	16
NiO-SDC	$La_{0.6}Sr_{0.4}Co_{0.8}Cu_{0.2}O_{3-\delta}$	SDC	550	490	17
Ni-GDC	$Ba_{0.6}Sr_{0.4}Co_{0.8}fE_{0.2}O_{3-\delta}$	GDC	550	863	18
Lithiated NiO	$Ni_{0.6}Cu_{0.4-x}Zn_xO$	SDC	600	624	19
Ni-NSDC	$Cu_{0.2}Zn_{0.8}$-NSDC	NSDC	550	1000	5
LiNiCuZn oxides-NSDC	LiNiCuZn oxides-NSDC	NSDC	470	1000	—

Compared with other kinds of electrodes listed in Table 4.1, the LiNiCuZn oxide exhibits a much better catalytic effect. With the exception of LiNiCuZn, the mixed electrode offers its best performance with Ni-NSDC as the anode and $Cu_{02}Zn_{08}$–

NSDC as the cathode, reaching 1000 mW/cm² at 550 °C [101]. As mentioned above, the LiNiCuZn oxide which was synthesized by the slurry method exhibits a much better electrochemical effect at low temperature compared with the traditional electrode of the SOFC and the other kinds of LTCOFC electrodes.

4.3.2 CO_2 and air mixture as oxidant (Publication IV)

The electrochemical performance of the LTSOFC/ceramic fuel cell with both air and air mixed with CO_2 as an oxidant were illustrated in Publication IV. The cells were produced using the hot-pressing method at 580 °C. A LiNiCuZn electrode and CSDC electrolyte were employed, made by co-precipitation synthesis and the hot-pressing fabrication method.

There are two kinds of fuel cell measurements in this experiment; both of the methods use H2 as a fuel and air, or a mixture of air and carbon dioxide, as an oxidant. The carbon dioxide and air was fully mixed before supplied to the cathode of the fuel cell; the carbon dioxide content was about 10–15% in the oxidant mixture.

In Fig. 4.20, the best CFC test cell provided an OCV of 1.2 V and a power density of 500 mW/cm² at 500 °C when mixed CO_2 with air as an oxidant. However, without the CO_2, the current and power density dropped considerably, which demonstrates the presence of the MCFC reactions. The highest OCV observed was 1.4 V, but this was followed by a lower maximum power density. Dropping the operational temperature to 400 °C significantly reduces the effect from CO_2, which is explained by the disappearance of the molten carbonate phase. High-temperature molten carbonates may reach a high OCV [24].

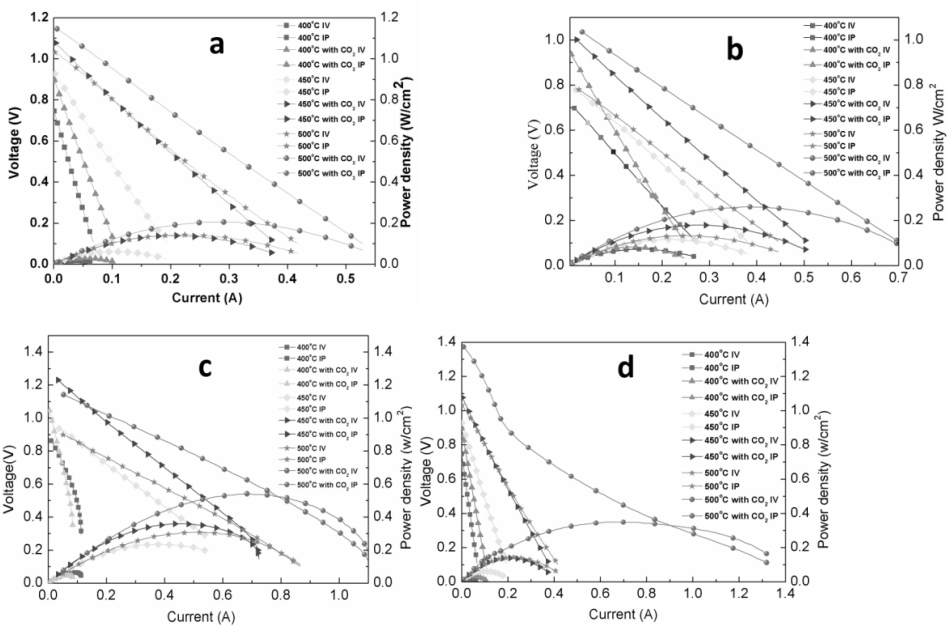

Figure 4.20. Comparison of the electrochemical performance of CFC with CSDC as an electrolyte at different temperatures and with/without CO_2 in the oxidant. (a), (b), (c), and (d) represent four different button fuel cells with similar kinds of electrolyte and electrode materials. Reproduced with permission from Publication IV. Copyright 2017 OneCentralPress.

The fact that several fuel cell reactions may be involved could also explain the higher voltage. In particular, when CO_2 is fed across the fuel cell according to the concentration contribution, it could affect the voltage through the Nernst equation?

In Fig. 4.20a and b, as the temperature increases, the enhancement of the electrochemical performance of the CO2 supply in the fuel cell is larger, especially when the temperature reached 500 ^{o}C; the enhancement reached 0.1–0.2V and 100 mW on voltage and power density.

In Fig. 4.20c and d, the performance of the fuel cells were similar with that of Fig. 4.20 a and b. However, the voltage of the fuel cell, which was fed with CO_2 and air as the oxidant, reached 1.3 V at 450 ^{o}C and 1.4 V at 500 ^{o}C separately, and the power density were notably enhanced. In high temperature molten carbonate salts, if a carbon/carbonate reaction occurred, an OCV of 1.51 V (steam) or 1.57 V (liquid) could in theory be possible (reactions: $CO_2+2H_2 \rightarrow C+2H_2O$ and

$2C+CO_3^{2-}-2e^- \rightarrow 3CO$), which is much higher than the theoretical OCV of 1.07V for a standard hydrogen-oxygen fuel cell at 500 °C [25-28]. We did not, however, observe direct deposition of carbon on the anode side. On the other hand, when several gases and ions are involved, one explanation could also be that the activities of the species involved through the Nernst equation [102].

4.3.3 Hot-pressed LTSOFC with CO_2 and air mixture as an oxidant

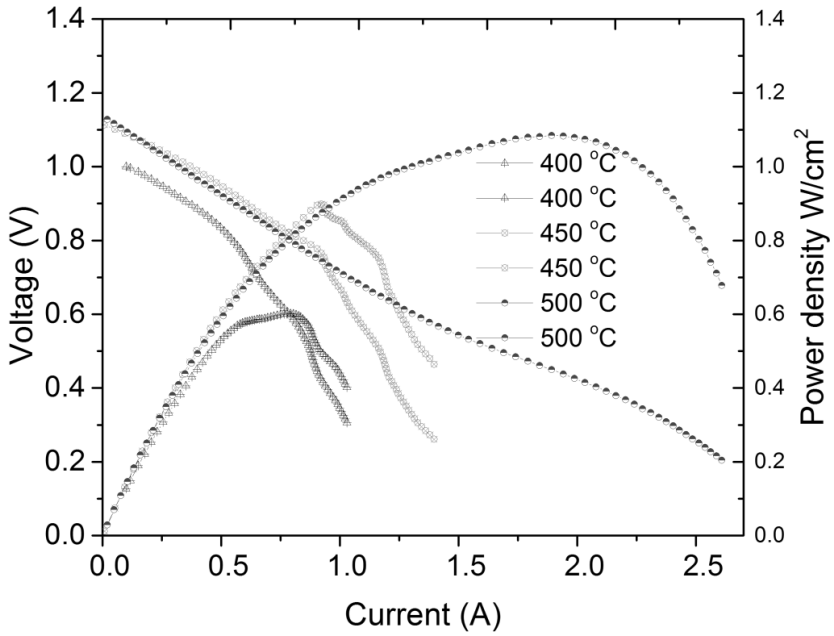

Figure 4.21. Electrochemical performance of a hot-pressed low temperature fuel cell made from electrolyte and electrode film with CO_2 and air mixture as an oxidant.

The low temperature nano-composite solid oxide fuel cell fabricated by the hot-pressing method was measured with H_2 as the fuel and CO_2 and air as the oxidant in Fig. 4.21. The electrolyte of LTSOFC was synthesized by the freeze-drying method with 30% carbonate content, and LiNiCuZn was prepared by the solid mixing method. The LTSOFC was fabricated by the hot-pressing method, the electrolyte and electrode films were pressed together at 580 °C into the LTSOFC under a 5 tons pressure.

The IV curves and I-P curves at 400–450 ^{o}C are not smooth. The wave shape rose and fell on it in Fig. 4.21 as the carbonate in the LTSOFC had not completely softened during the carbonate softening temperature [67, 88]. In the LTSOFC in Fig. 4.21, due to the incomplete carbonate softening, the ionic resistance of the LTSOFC is too high and insufficient free CO_3^{2-} caused a steep drop in voltage with increasing current. The IV and IP curves spread in a smooth way when the operating temperature reached 500 ^{o}C when the alkali carbonate completely softened. The current of the LTSOFC was extremely enhanced when the carbonate softening was completed along with the effect from CO_2 in the oxidant. The fuel cell power density reached about 1.1 W/cm^2 at 500 ^{o}C, which is higher than the performance of the LTSOFC in Fig. 4.19. The OCV of the LTSOFC in Fig. 4.21 reached 1.13 Volt at 500 ^{o}C, which is higher than 1 V reached by the OCV in Fig. 4.19 when the fuel cell was operated at 470 ^{o}C.

5. Summary and conclusions

In this thesis, several different methods were investigated for material synthesis for low-temperature solid oxide fuel cells. The effects of oxidant content and fuel cell fabrication were also analyzed.

LiNiCuZn was utilized as the main electrode material, and it was synthesized with the slurry and solid mixing methods. For the electrolyte materials, SDC or CSDC were used and synthesized through co-precipitation, freeze-drying, and spark plasma sintering methods. Material synthesis was accompanied by an electrochemical analysis of the ionic conductivity and fuel cell performance. In addition, a comprehensive characterization of materials was accomplished.

As to the whole fuel cell performance, a notable result was achieved with an LTSOFC design which comprised of a LiNiCuZn electrode synthesized by the slurry mixing method and an NSDC electrolyte prepared by the co-precipitation method. The highest power density reached was 1000 mW/cm^2 at 470 ^{o}C which is better than that found in previous studies, as shown in Table 4.1, which achieved the same performance value but at a higher temperature of 500 ^{o}C.

A comparison of the different methods for synthesizing the electrolyte material illustrated that with the freeze-drying method, a high ionic conductivity of 400 mS/cm was achieved with CSDC, which is much better than that of NSDC synthesized by co-precipitation. In the freeze-drying method, the carbonate and the SDC mix is in a liquid state instead of a solid state in the co-precipitation method, which increases the size and uniformity of the interface between the carbonate and SDC.

With the SPS method, an ionic conductivity of 430 mS/cm for CSDC was reached. The SPS method produces a very dense electrolyte, which in turn

reduces the volume of gas between particles and increases the carbonate content, which is beneficial to ionic conductivity. However, using the SPS-based electrolyte in a whole fuel cell configuration is not easy, because it is thin and breaks easily. Further work on SPS could include optimization of the cell fabrication thickness.

Comparing freeze-drying to the co-precipitation methods indicated that the former offered a much better ionic conductivity of the electrolyte, easy control of the carbonate content, and more uniform mixing of the carbonate and SDC elements. These benefits were turned into a better overall fuel cell performance which reached 1.1 W/cm2 at 500 ^{o}C.

In terms of preparing the whole fuel cell from powders, the cold-pressing method yielded an outstanding fuel cell electrochemical performance in several instances. However, on average, the cells performed worse than that with hot pressing, and the cells were also very fragile.

When using a carbonate in the electrolyte, it will also add the carbonate ion to the ionic conductivity through similar processes as in the MCFC fuel cell. Adding CO_2 to the air oxidant in the CSDC-based LTSOFC enhanced the fuel cell performance compared to air only. The power density was improved by 30–100% and the OCV by 0.1–0.2 V. An OCV up to 1.3–1.4 V was measured with an O_2 + CO_2 mixture at a temperature below 500 ^{o}C explained by the MCFC-type of effects. The overall fuel cell performance remained, however, below the best fuel cell reported in this thesis.

The best electrochemical performance of the LTSOFC was achieved when applying the freeze-drying synthesis method, hot-pressing fabrication, and CO2 mixed into air as an oxidant. Compared with the LTSOFC using the cold-pressing method with co-precipitation method prepared electrolyte, the hot-pressed film LTSOFC with a freeze-drying synthesis electrolyte has better electrochemical performance, higher stability, and higher yield, but its preparation requires more time.

As a next step, it is recommended to work on the electrode and electrolyte coupling and interfacing, in particular with the electrolyte material fabricated by

the freeze-drying method to yield a high ionic conductivity, high OCV, and increased power density. The experimental set-up and manufacturing of the test fuel cells turned out to be quite challenging and attractive. Further work on standardizing the fuel cell manufacturing processes would be highly motivating.

References

[1] Qureshi, M. I., Rasli, A. M., Zaman, K. (2016) Journal of Cleaner Production 112, 3657–3666.

[2] Chinnammai, S., (2014) International Journal of Environmental Science and Development 5, 404-411.

[3] Bordoloi, N. K., Rai, S. K., Chaudhuri, M. K., Mukherjee, K. A. (2014) Fuel Processing Technology 119, 236–244.

[4] Ferry, R., Monoian, E. A field guide to renewable energy technologies. 2012.

[5] How Tesla will change the world, 2015. http://waitbutwhy.com/2015/06/how-tesla-will-change-your-life.html.

[6] Pang, R., Deng, Z., Hu, J. (2015) Renewable and Sustainable Energy Reviews 52, 1158–1171.

[7] Huang, M. H., Yang, H. W., Chen, D. Z. (2015) Journal of Informetrics 9(2), 237–249.

[8] Minh, N. Q., Takahashi, T. (1995) Science and Technology of Ceramic Fuel Cells, Elsevier Ltd. 379pp.

[9] Fuel cell today. 2012. http://www.fuelcelltoday.com/media/1587227/fuel_cells_and_hydrogen_in_china_2012.pdf

[10] Warshay, M., Paul, R. 1989. http://ntrs.nasa.gov/archive/nasa/casi.ntrs.nasa.gov/19900002488.pdf.

[11] Krummrich, S., Llabrés, J. (2015) International Journal of Hydrogen Energy 40, 5482–5486.

[12] Singhal, S. C. (2007) Electrochemical Society Interface 42-44.

[13] Baldinelli, A., Barelli, L., Bidini, G. (2015) Energy 90(2), 2070–2084.

[14] Eguchi, K., Kojob, H., Takeguchi, T., Kikuchi, R., Sasaki, K. (2002) Solid State Ionics 152, 411 – 416.

[15] Kariya, T., Tanaka, H., Hirono, T., Kuse, T., Yanagimoto, K., Uchiyama, K., Henmi, M., Hirose, M., Kimura, I., Suu, K., Funakubo, H. (2016) Journal of Alloys and Compounds 654, 171–175.

[16] Zhu, Z., Sun, W., Shi, Z., Liu, W. (2016) Journal of Alloys and Compounds 658, 716 – 720.

[17] Hou, J., Liu, F., Gong, Z., Wu, Y., Liu, W. (2015) Journal of Power Sources 299, 32–39.

[18] Hou, J., Bi, L., Qian, J., Gong, Z., Zhu, Z., Liu, W. (2016) Journal of Power Sources 301, 306–311.

[19] Bae, J., Lee, D., Hong, S., Yang, H., Kim, Y. (2015) Surface and Coatings Technology 279, 54–59.

[20] Khan, M. Z., Song, R., Lee, S., Lee, J., Lim, T., Park, S. (2014) International Journal of Hydrogen Energy 39(35), 20799–20805.

[21] Wang, Z., Li, Y., Schwank, J. W. (2014) Journal of Power Sources 248, 239–245.

[22] Ma, Y., Wang, X., Khalifa, H. A., Zhu, B., Muhammed, M. (2012) International Journal of Hydrogen Energy 37(24), 19401–19406.

[23] Zhao, Y., Xia, C., Jia, L., Wang, Z., Li, H., Yu, J., Li, Y. (2013) International Journal of Hydrogen Energy 38, 16498-16517.

[24] Gao, Z., Mao, Z., Wang, C., Liu, Z.(2010) International Journal of Hydrogen Energy 35, 12897–12904.

[25] Nagasawa, T., Hanamura, K. (2015) Journal of Power Sources 290, 168–182.

[26] Ramani, V. (2006) Fuel cells. Electrochemical Society Interface.

[27] How does the Fuel Cell Work? http://batteryuniversity.com/learn/article/fuel_cell_technology.

[28] Torabi, A., Etsell, T. H., Sarka, P. (2011) Solid State Ionics 192(1), 372–375.

[29] Zhou, J., Chen, Y., Chen, G., Wu, K., Cheng, Y. (2015) Journal of Alloys and Compounds 647, 778–783

[30] Hua, C., Chou, C. (2015) Ceramics International 41, 1708–1712.

[31] Heusing, S., Aegerter, M. A. (2012) Springer US. 239-274.

[32] Williams, M. C. (200) Fuel Cell Handbook. EG&G Technical Services, Inc. 427pp.

[33] Haj-Kacem, R.B., Ouerfelli, N., Herráez, J.V., Guettari, M., Hamda, H., Dallel, M. (2014) Fluid Phase Equilibria 383, 11–20.

[34] Fuel cells. 2004, http://www.understandingchp.com/appguide/chapters/chap4/4-4_fuel_cells.htm.

[35] Harris, J.A., Collings, N. (2015) Sensors and Actuators B: Chemical 221, 81–87.

[36] Zhu, H., Kee, R. J. (2016) International Journal of Hydrogen Energy 41(4), 2931–2943.

[37] Singhal, S.C., Kendall, K. (2003) Solid oxide fuel cells. ISBN 1-85617-387-9.

[38] The main types of fuel cell technology 2010. http://www.cleantechinvestor.com/portal/fuel-cells/6426-the-main-types-of-fuel-cell-technology.html.

[39] Cifrain, M., Kordesch, K. (2003) Handbook of Fuel Cells – Fundamentals, Technology and Applications. 267-280.

[40] Alesker, M., Page, M., Shviro, M., Paska, Y., Gershinsky, G., Dekel, D. R., Zitoun, D. (2016) Journal of Power Sources 304, 332–339.

[41] Rayment, C., Sherwin, S. Dame. N. IN, (2003) 46556, 11-12.

[42] Alkaline Fuel Cell – AFC. http://www.ogniwa-paliwowe.info/afc.php.

[43] Kamal, R., Rasheed, A., Chan, S. H. (2015) Applied Energy 140, 44–51.

[44] Ramiar, A., Mahmoudi, A.H., Esmaili, Q., Abdollahzadeh, M. (2016) Energy 94, 206–217.

[45] Guan, T., Chutichai, B., Alvfors, P. A. (2015) Energy Conversion and Management 106, 1183–1191.

[46] Moreno, N. G., Molina, M. C., Gervasio, D., Francisco, J., Robles, P. (2015) Renewable and Sustainable Energy Reviews 52, 897–906.

[47] Wang, Y., Chen, K. S., Mishler, J., Choa, S. C., Adroher, X. C. (2011) Applied Energy 88, 981–1007.

[48] Fuel Cell Basics. http://americanhistory.si.edu/fuelcells/basics.htm.

[49] Choudhury, S. R., Choudhury, S. R., Rangarajan, J., Rengaswamy, R. (2005) Journal of Power Sources 140(2), 274–279.

[50] Phosphoric Acid Fuel Cells.

http://scopewe.com/category/chemical-engineering/fuel-cell/.

[51] Baronci, A., Messina, G., McPhail, S. J., Moreno, A. (2015) Energy 93, 1063–1073.

[52] Garrison, E. Solid Oxide Fuel Cells. http://mypages.iit.edu/~smart/garrear/fuelcells.htm.

[53] Halliop, W., Tuck, A., Thompson, W. T. (2005) the Electrochemical Society. 191.

[54] Solid Oxide Fuel Cell Technology. http://www.protonex.com/technology/solid-oxide-fuel-cell/.

[55] Rahmawati, F., Fajriati, W., Heraldy, E., Syarif, D. G. (2015) Procedia Chemistry 14,164–170.

[56] Courtin, E., Boy, P., Piquero, T., Vulliet, J., Poirot, N., Laberty-Robert, C. (2012) Journal of Power Sources 206, 77-83.

[57] Zhao, Y., Xiong, D., Qin, H., Gao, F., Inui, H., Zhu, B. (2012) International Journal of Hydrogen Energy 37(24), 19351–19356.

[58] Andrew, S., Martinez, J., Brouwer, G., Samuelsen, S. (2015) Applied Energy 148, 421–438.

[59] Zhu, B. (2009) International Journal of Energy Research 33, 1126/1137.

[60] Baronci, A., Messina, G., McPhail, S. J., Moreno. A. (2015) Energy 93, 1063–1073.

[61] Swatsitang, E., Phokha, S., Hunpratub, S., Maensiri, S. (2016) Physica B: Condensed Matter 485, 14–20.

[62] Li,Y., Rui, Z., Xia, C., Anderson. M, Lin. Y.S. (2009) Catalysis Today 148(3–4), 303–309.

[63] Zhu, B., Li, S., Mellander, B. E. (2008) Electrochemistry Communications 10, 302-305.

[64] Wang, X., Ma, Y., Raza, R., Muhammed, M., Zhu, B. (2008) Electrochemistry Communications 10, 1617-1620.

[65] Wang, X., Ma, Y., Li, S., Kashyout, A., Zhu, B., Muhammed, M. (2011) Journal of Power Sources 196, 2754-2758.

[66] Zhu, B., Mat, MD. (2006) International Journal of Electrochemical Sciences 1, 383-402.

[67] Zhu, B., Fan, L., Lund, P. (2013) Applied Energy 106, 163–175.

[68] Zhu, B. (2011) J. Nanosci. Nanotechnology 11, 8873-8879.

[69] Wang, X., Ma, Y. Li., S. (2008) Electrochemistry Communications 10 (10) 1617-1620.

[70] Cheng, J ., Deng, L., Zhang, B., Shi, P., Meng, G. (2007) Rare Metals 26(2), 110–117.

[71] Liu, M., Kleij, A. van der., Verkooijen, A.H.M., P.V. Aravind. (2013) Applied Energy 108, 149–157

[72] Fu, C. J., Sun, K. N., Chen, X. B., Zhang, N. Q., Zhou, D. R. (2009) Electrochemistry communications 54, 7305.

[73] Kravchyk, K. V., Bohnke, O., Gunes, V., Belous, A. G., Pashkova, E. V., Lannic, J. L., Gouttefangeas, F. (2012) Solid State Ionics 226, 53–58.

[74] Ma, Y., Wang, X., Khalifa, H. A., Zhu, B., Muhammed, M. (2012) International Journal of Hydrogen Energy 37(24), 19401–19406

[75] Chen, D., Zhang, Q., Lu, L., Periasamy, V., Tade, M. O., Shao, Z. (2016) Journal of Power Sources 303, 305–316.

[76] Baronci, A., Messina, G., McPhail, S. J., Moreno. A. (2015) Energy 93, 1063–1073.

[77] Jing, Y., Ma, Y., Patakangas, J., Zhu, B., Johnsson, M., Cura, M. E., Lund, P. (2014) International Journal of Hydrogen Energy 39(26), 14391– 14396.

[78] Zhu, B., Liu, X., Zhu, Z., Ljungberg, R. (2006) American Society of Mechanical Engineers 973-976.

[79] Baral, A. K., Dasari, H. P., Kim, B., Lee, J. (2013) Journal of Alloys Compounds 575, 455–460.

[80] Mackie, A. J., Hatton G. D., Hamilton, H. G. C., Dean, J. S., Goodall, R.（2016）Materials Letters 171, 14–17.

[81] Thermal technology LLC, Spark Plasma Sintering (SPS/DCS) (2009)

http://www.thermaltechnology.com/spark-plasma-sintering.html

[82] Hui, S., Roller, J., Yick, S., Zhang, X., Deces-Petit, C., Xie, Y., Maric, R., Ghosh, D. J. (2007) Journal of Power Sources 172, 493.

[83] Schouler, E., Mesbahi, N., Vitter, G. (1983) Solid State Ionics 9-10:989-996.

[84] Ding, C., Sato, K., Mizusaki, J., Hashida, T. (2012) Ceramics International 38, 85–92.

[85] Jing, Y., Qin, H., Liu, Q., Singh, M., Zhu, B. (2012) Journal of Nanoscience and Nanotechnology 12, 1–4.

[86] Patakangas, J., Ma, Y., Jing, Y., Lund, P. (2014) Journal of Power Sources 263, 315-331

[87] Zhou, Z., Kato, K., Komaki, T., Yoshino, M., Yukawa, H., Morinaga, M., Morita, K., Eur, J. (2004) Journal of the American Ceramic Society 24, 139.

[88] Lapa, C., Figueiredo, F, .Souza, D. D., Song, L., Zhu, B., Marques, F. (2010) International Journal of Hydrogen Energy 35. 2953-2957.

[89] Xia, C., Li, Y., Tian, Y., Liu, Q., Wang, Z., Jia, L. (2010) Journal of Power Sources 195, 3149-3154.

[90] Ferreira, ASV., Soares, CMC, Figueiredo, LR., Marques, FMB. (2011) International Journal of Hydrogen Energy 36, 3704-3711.

[91] Xia, C., Li, Y., Tian, Y., Liu, Q., Zhao, Y., Jia, L. (2009) Journal of Power Sources188, 156-162.

[92] Fan, L., Wang, C., Di, J., Chen, M., Zheng, J., Zhu, B. (2012) Journal of Nanoscience and Nanotechnology 12, 4941-4945.

[93] Li, X., Xiao, G., Huang, K. (2011) Journal of the Electrochemical Society 158 (2), 225-232.

[94] Di, J., Chen, M., Wang, C., Zheng, J., Fan, L., Zhu, B. (2010) Journal of Power Sources 195, 4695-4699.

[95] Wang, X., Ma, Y., Raza, R., Muhammed, M., Zhu, B. (2008) Electrochemistry Communications 10(10), 1617-1620.

[96] Saradha, T., Fereira, AS., Patricio, SG., Figueiredo, FML., Marques, FMB. (2012) International Journal of Hydrogen Energy 37(8), 7235-7241.

[97] Raza, R., Qin, H., Fan, L., Takeda, K., Mizuhata, M., Zhu, B. (2012) Journal of Power Sources 201, 121-127.

[98] Huang, K., Mao, Z., Liu, Z., Wang, C. (2007) Electrochemistry Communication 9, 2601-2605.

[99] Zuo, C., Zha, S., Liu, M., Hatano, M., Uchiyama, M. (2006) Advanced Materials 18(24), 3318-3320.

[100] Wang, X., Ma, Y., Li, S., Kashyout, A., Zhu, B., Muhammed, M. (2011) Journal of Power Sources 196(5), 2754-2758.

[101] Raza, R., Wang, X. D., Ma, Y., Zhu, B. (2010) Journal of Power Sources 195, 6491.

[102] Blomen, M. J., Mugerwa, M. N. (1993) Fuel cell systems. Plenum Press, New York.

The teacher opens the door. You enter by yourself.
Old Chinese proverb

Aalto-DD 138/2017

ISBN 978-952-60-7538-9 (printed)
ISBN 978-952-60-7537-2 (pdf)
ISSN-L 1799-4934
ISSN 1799-4934 (printed)
ISSN 1799-4942 (pdf)

Aalto University
School of Science
Department of Applied Physics
www.aalto.fi